Measurement of branching fractions for exclusive *B* decays to charmonium final states

B. Aubert, D. Boutigny, J.-M. Gaillard, A. Hicheur, Y. Karyotakis, J. P. Lees, P. Robbe, and V. Tisserand
Laboratoire de Physique des Particules, F-74941 Annecy-le-Vieux, France

A. Palano
Università di Bari, Dipartimento di Fisica and INFN, I-70126 Bari, Italy

G. P. Chen, J. C. Chen, N. D. Qi, G. Rong, P. Wang, and Y. S. Zhu
Institute of High Energy Physics, Beijing 100039, China

G. Eigen, P. L. Reinertsen, and B. Stugu
University of Bergen, Institute of Physics, N-5007 Bergen, Norway

B. Abbott, G. S. Abrams, A. W. Borgland, A. B. Breon, D. N. Brown, J. Button-Shafer, R. N. Cahn, A. R. Clark, M. S. Gill, A. Gritsan, Y. Groysman, R. G. Jacobsen, R. W. Kadel, J. Kadyk, L. T. Kerth, S. Kluth, Yu. G. Kolomensky, J. F. Kral, C. LeClerc, M. E. Levi, T. Liu, G. Lynch, A. Meyer, M. Momayezi, P. J. Oddone, A. Perazzo, M. Pripstein, N. A. Roe, A. Romosan, M. T. Ronan, V. G. Shelkov, A. V. Telnov, and W. A. Wenzel
Lawrence Berkeley National Laboratory and University of California, Berkeley, California 94720

P. G. Bright-Thomas, T. J. Harrison, C. M. Hawkes, A. Kirk, D. J. Knowles, S. W. O'Neale, R. C. Penny, A. T. Watson, and N. K. Watson
University of Birmingham, Birmingham, B15 2TT, United Kingdom

T. Deppermann, K. Goetzen, H. Koch, J. Krug, M. Kunze, B. Lewandowski, K. Peters, H. Schmuecker, and M. Steinke
Ruhr Universität Bochum, Institut für Experimentalphysik 1, D-44780 Bochum, Germany

J. C. Andress, N. R. Barlow, W. Bhimji, N. Chevalier, P. J. Clark, W. N. Cottingham, N. De Groot, N. Dyce, B. Foster, J. D. McFall, D. Wallom, and F. F. Wilson
University of Bristol, Bristol BS8 1TL, United Kingdom

K. Abe, C. Hearty, T. S. Mattison, J. A. McKenna, and D. Thiessen
University of British Columbia, Vancouver, BC, Canada V6T 1Z1

S. Jolly, A. K. McKemey, and J. Tinslay
Brunel University, Uxbridge, Middlesex UB8 3PH, United Kingdom

V. E. Blinov, A. D. Bukin, D. A. Bukin, A. R. Buzykaev, V. B. Golubev, V. N. Ivanchenko, A. A. Korol, E. A. Kravchenko, A. P. Onuchin, A. A. Salnikov, S. I. Serednyakov, Yu. I. Skovpen, V. I. Telnov, and A. N. Yushkov
Budker Institute of Nuclear Physics, Novosibirsk 630090, Russia

D. Best, A. J. Lankford, M. Mandelkern, S. McMahon, and D. P. Stoker
University of California at Irvine, Irvine, California 92697

A. Ahsan, K. Arisaka, C. Buchanan, and S. Chun
University of California at Los Angeles, Los Angeles, California 90024

J. G. Branson, D. B. MacFarlane, S. Prell, Sh. Rahatlou, G. Raven, and V. Sharma
University of California at San Diego, La Jolla, California 92093

C. Campagnari, B. Dahmes, P. A. Hart, N. Kuznetsova, S. L. Levy, O. Long, A. Lu, J. D. Richman, W. Verkerke, M. Witherell, and S. Yellin
University of California at Santa Barbara, Santa Barbara, California 93106

J. Beringer, D. E. Dorfan, A. M. Eisner, A. Frey, A. A. Grillo, M. Grothe, C. A. Heusch, R. P. Johnson, W. Kroeger, W. S. Lockman, T. Pulliam, H. Sadrozinski, T. Schalk, R. E. Schmitz, B. A. Schumm, A. Seiden, M. Turri, W. Walkowiak, D. C. Williams, and M. G. Wilson
University of California at Santa Cruz, Institute for Particle Physics, Santa Cruz, California 95064

E. Chen, G. P. Dubois-Felsmann, A. Dvoretskii, D. G. Hitlin, S. Metzler, J. Oyang, F. C. Porter, A. Ryd, A. Samuel,

M. Weaver, S. Yang, and R. Y. Zhu
California Institute of Technology, Pasadena, California 91125

S. Devmal, T. L. Geld, S. Jayatilleke, G. Mancinelli, B. T. Meadows, and M. D. Sokoloff
University of Cincinnati, Cincinnati, Ohio 45221

T. Barillari, P. Bloom, M. O. Dima, S. Fahey, W. T. Ford, D. R. Johnson, U. Nauenberg, A. Olivas, H. Park, P. Rankin, J. Roy, S. Sen, J. G. Smith, W. C. van Hoek, and D. L. Wagner
University of Colorado, Boulder, Colorado 80309

J. Blouw, J. L. Harton, M. Krishnamurthy, A. Soffer, W. H. Toki, R. J. Wilson, and J. Zhang
Colorado State University, Fort Collins, Colorado 80523

T. Brandt, J. Brose, T. Colberg, G. Dahlinger, M. Dickopp, R. S. Dubitzky, E. Maly, R. Müller-Pfefferkorn, S. Otto, K. R. Schubert, R. Schwierz, B. Spaan, and L. Wilden
Technische Universität Dresden, Institut für Kern- und Teilchenphysik, D-01062, Dresden, Germany

L. Behr, D. Bernard, G. R. Bonneaud, F. Brochard, J. Cohen-Tanugi, S. Ferrag, E. Roussot, S. T'Jampens, C. Thiebaux, G. Vasileiadis, and M. Verderi
Ecole Polytechnique, F-91128 Palaiseau, France

A. Anjomshoaa, R. Bernet, A. Khan, F. Muheim, S. Playfer, and J. E. Swain
University of Edinburgh, Edinburgh EH9 3JZ, United Kingdom

M. Falbo
Elon College, Elon College, North Carolina 27244-2010

C. Borean, C. Bozzi, S. Dittongo, M. Folegani, and L. Piemontese
Università di Ferrara, Dipartimento di Fisica and INFN, I-44100 Ferrara, Italy I-44100 Ferrara, Italy

E. Treadwell
Florida A&M University, Tallahassee, Florida 32307

F. Anulli,* R. Baldini-Ferroli, A. Calcaterra, R. de Sangro, D. Falciai, G. Finocchiaro, P. Patteri, I. M. Peruzzi,* M. Piccolo, Y. Xie, and A. Zallo
Laboratori Nazionali di Frascati dell'INFN, I-00044 Frascati, Italy

S. Bagnasco, A. Buzzo, R. Contri, G. Crosetti, P. Fabbricatore, S. Farinon, M. Lo Vetere, M. Macri, M. R. Monge, R. Musenich, M. Pallavicini, R. Parodi, S. Passaggio, F. C. Pastore, C. Patrignani, M. G. Pia, C. Priano, E. Robutti, and A. Santroni
Università di Genova, Dipartimento di Fisica and INFN, I-16146 Genova, Italy

M. Morii
Harvard University, Cambridge, Massachusetts 02138

R. Bartoldus, T. Dignan, R. Hamilton, and U. Mallik
University of Iowa, Iowa City, Iowa 52242

J. Cochran, H. B. Crawley, P.-A. Fischer, J. Lamsa, W. T. Meyer, and E. I. Rosenberg
Iowa State University, Ames, Iowa 50011-3160

M. Benkebil, G. Grosdidier, C. Hast, A. Höcker, H. M. Lacker, V. LePeltier, A. M. Lutz, S. Plaszczynski, M. H. Schune, S. Trincaz-Duvoid, A. Valassi, and G. Wormser
Laboratoire de l'Accélérateur Linéaire, F-91898 Orsay, France

R. M. Bionta, V. Brigljević, D. J. Lange, M. Mugge, X. Shi, K. van Bibber, T. J. Wenaus, D. M. Wright, and C. R. Wuest
Lawrence Livermore National Laboratory, Livermore, California 94550

M. Carroll, J. R. Fry, E. Gabathuler, R. Gamet, M. George, M. Kay, D. J. Payne, R. J. Sloane, and C. Touramanis
University of Liverpool, Liverpool L69 3BX, United Kingdom

M. L. Aspinwall, D. A. Bowerman, P. D. Dauncey, U. Egede, I. Eschrich, N. J. W. Gunawardane, J. A. Nash, P. Sanders, and D. Smith
University of London, Imperial College, London, SW7 2BW, United Kingdom

D. E. Azzopardi, J. J. Back, P. Dixon, P. F. Harrison, R. J. L. Potter, H. W. Shorthouse, P. Strother, P. B. Vidal, and M. I. Williams
Queen Mary, University of London, E1 4NS, United Kingdom

G. Cowan, S. George, M. G. Green, A. Kurup, C. E. Marker, P. McGrath, T. R. McMahon, S. Ricciardi, F. Salvatore, I. Scott, and G. Vaitsas
University of London, Royal Holloway and Bedford New College, Egham, Surrey TW20 0EX, United Kingdom

D. Brown and C. L. Davis
University of Louisville, Louisville, Kentucky 40292

J. Allison, R. J. Barlow, J. T. Boyd, A. C. Forti, J. Fullwood, F. Jackson, G. D. Lafferty, N. Savvas, E. T. Simopoulos, and J. H. Weatherall
University of Manchester, Manchester M13 9PL, United Kingdom

A. Farbin A. Jawahery, V. Lillard, J. Olsen, D. A. Roberts, and J. R. Schieck
University of Maryland, College Park, Maryland 20742

G. Blaylock, C. Dallapiccola, K. T. Flood, S. S. Hertzbach, R. Kofler, T. B. Moore, H. Staengle, and S. Willocq
University of Massachusetts, Amherst, Massachusetts 01003

B. Brau, R. Cowan, G. Sciolla, F. Taylor, and R. K. Yamamoto
Massachusetts Institute of Technology, Lab for Nuclear Science, Cambridge, Massachusetts 02139

M. Milek, P. M. Patel, and J. Trischuk
McGill University, Montréal, QC, Canada H3A 2T8

F. Lanni and F. Palombo
Università di Milano, Dipartimento di Fisica and INFN, I-20133 Milano, Italy

J. M. Bauer, M. Booke, L. Cremaldi, V. Eschenburg, R. Kroeger, J. Reidy, D. A. Sanders, and D. J. Summers
University of Mississippi, University, Mississippi 38677

J. P. Martin, J. Y. Nief, R. Seitz, P. Taras, and V. Zacek
Université de Montréal, Lab. Rene J. A. Levesque, Montréal, QC, Canada H3C 3J7

H. Nicholson and C. S. Sutton
Mount Holyoke College, South Hadley, Massachusetts 01075

C. Cartaro, N. Cavallo,[†] G. De Nardo, F. Fabozzi, C. Gatto, L. Lista, P. Paolucci, D. Piccolo, and C. Sciacca
Università di Napoli Federico II, Dipartimento di Scienze Fisiche and INFN, I-80126, Napoli, Italy

J. M. LoSecco
University of Notre Dame, Notre Dame, Indiana 46556

J. R. G. Alsmiller, T. A. Gabriel, and T. Handler
Oak Ridge National Laboratory, Oak Ridge, Tennessee 37831

J. Brau, R. Frey, M. Iwasaki, N. B. Sinev, and D. Strom
University of Oregon, Eugene, Oregon 97403

F. Colecchia, F. Dal Corso, A. Dorigo, F. Galeazzi, M. Margoni, G. Michelon, M. Morandin, M. Posocco, M. Rotondo, F. Simonetto, R. Stroili, E. Torassa, and C. Voci
Università di Padova, Dipartimento di Fisica and INFN, I-35131 Padova, Italy

M. Benayoun, H. Briand, J. Chauveau, P. David, C. De la Vaissière, L. Del Buono, O. Hamon, F. Le Diberder, Ph. Leruste, J. Lory, L. Roos, J. Stark, and S. Versillé
Universités Paris VI et VII, LPNHE, F-75252 Paris, France

P. F. Manfredi, V. Re, and V. Speziali
Università di Pavia, Dipartimento di Elettronica and INFN, I-27100 Pavia, Italy

E. D. Frank, L. Gladney, Q. H. Guo, and J. H. Panetta
University of Pennsylvania, Philadelphia, Pennsylvania 19104

C. Angelini, G. Batignani, S. Bettarini, M. Bondioli, M. Carpinelli, F. Forti, M. A. Giorgi, A. Lusiani, F. Martinez-Vidal, M. Morganti, N. Neri, E. Paoloni, M. Rama, G. Rizzo, F. Sandrelli, G. Simi, G. Triggiani, and J. Walsh
Università di Pisa, Scuola Normale Superiore and INFN, I-56010 Pisa, Italy

M. Haire, D. Judd, K. Paick, L. Turnbull, and D. E. Wagoner
Prairie View A&M University, Prairie View, Texas 77446

J. Albert, C. Bula, P. Elmer, C. Lu, K. T. McDonald, V. Miftakov, S. F. Schaffner, A. J. S. Smith, A. Tumanov, and E. W. Varnes
Princeton University, Princeton, New Jersey 08544

G. Cavoto, D. del Re, F. Ferrarotto, F. Ferroni, K. Fratini, E. Lamanna, E. Leonardi, M. A. Mazzoni, S. Morganti, G. Piredda, F. Safai Tehrani, M. Serra, and C. Voena
Università di Roma La Sapienza, Dipartimento di Fisica and INFN, I-00185 Roma, Italy

R. Faccini
University of California at San Diego, La Jolla, California 92093
and Università di Roma La Sapienza, Dipartimento di Fisica and INFN, I-00185 Roma, Italy

S. Christ and R. Waldi
Universität Rostock, D-18051 Rostock, Germany

T. Adye, B. Franek, N. I. Geddes, G. P. Gopal, and S. M. Xella
Rutherford Appleton Laboratory, Chilton, Didcot, Oxon, OX11 0QX, United Kingdom

R. Aleksan, G. De Domenico, S. Emery, A. Gaidot, S. F. Ganzhur, P.-F. Giraud, G. Hamel de Monchenault, W. Kozanecki, M. Langer, G. W. London, B. Mayer, B. Serfass, G. Vasseur, C. Yeche, and M. Zito
DAPNIA, Commissariat à l'Energie Atomique/Saclay, F-91191 Gif-sur-Yvette, France

N. Copty, M. V. Purohit, H. Singh, and F. X. Yumiceva
University of South Carolina, Columbia, South Carolina 29208

I. Adam, P. L. Anthony, D. Aston, K. Baird, E. Bloom, A. M. Boyarski, F. Bulos, G. Calderini, R. Claus, M. R. Convery, D. P. Coupal, D. H. Coward, J. Dorfan, M. Doser, W. Dunwoodie, R. C. Field, T. Glanzman, G. L. Godfrey, S. J. Gowdy, P. Grosso, T. Himel, M. E. Huffer, W. R. Innes, C. P. Jessop, M. H. Kelsey, P. Kim, M. L. Kocian, U. Langenegger, D. W. G. S. Leith, S. Luitz, V. Luth, H. L. Lynch, H. Marsiske, S. Menke, R. Messner, K. C. Moffeit, R. Mount, D. R. Muller, C. P. O'Grady, M. Perl, S. Petrak, H. Quinn, B. N. Ratcliff, S. H. Robertson, L. S. Rochester, A. Roodman, T. Schietinger, R. H. Schindler, J. Schwiening, V. V. Serbo, A. Snyder, A. Soha, S. M. Spanier, J. Stelzer, D. Su, M. K. Sullivan, H. A. Tanaka, J. Va'vra, S. R. Wagner, A. J. R. Weinstein, W. J. Wisniewski, D. H. Wright, and C. C. Young
Stanford Linear Accelerator Center, Stanford, California 94309

P. R. Burchat, C. H. Cheng, D. Kirkby, T. I. Meyer, and C. Roat
Stanford University, Stanford, California 94305-4060

R. Henderson
TRIUMF, Vancouver, BC, Canada V6T 2A3

W. Bugg, H. Cohn, and A. W. Weidemann

University of Tennessee, Knoxville, Tennessee 37996

J. M. Izen, I. Kitayama, X. C. Lou, and M. Turcotte
University of Texas at Dallas, Richardson, Texas 75083

F. Bianchi, M. Bona, B. Di Girolamo, D. Gamba, A. Smol, and D. Zanin
Università di Torino, Dipartimento di Fisica Sperimentale and INFN, I-10125 Torino, Italy

L. Lanceri, A. Pompili, and G. Vuagnin
Università di Trieste, Dipartimento di Fisica and INFN, I-34127 Trieste, Italy

R. S. Panvini
Vanderbilt University, Nashville, Tennessee 37235

C. M. Brown, A. De Silva, R. Kowalewski, and J. M. Roney
University of Victoria, Victoria, BC, Canada V8W 3P6

H. R. Band, E. Charles, S. Dasu, F. Di Lodovico, A. M. Eichenbaum, H. Hu, J. R. Johnson, R. Liu, J. Nielsen, Y. Pan, R. Prepost, I. J. Scott, S. J. Sekula, J. H. von Wimmersperg-Toeller, S. L. Wu, Z. Yu, and H. Zobernig
University of Wisconsin, Madison, Wisconsin 53706

T. M. B. Kordich and H. Neal
Yale University, New Haven, Connecticut 06511

(BABAR Collaboration)
(Received 11 July 2001; published 7 January 2002)

We report branching fraction measurements for exclusive decays of charged and neutral B mesons into two-body final states containing a charmonium meson. We use a sample of 22.72 ± 0.36 million $B\overline{B}$ events collected between October 1999 and October 2000 with the *BABAR* detector at the PEP-II storage rings at the Stanford Linear Accelerator Center. The charmonium mesons considered here are J/ψ, $\psi(2S)$, and χ_{c1}, and the light meson in the decay is either a K, K^*, or π^0.

DOI: 10.1103/PhysRevD.65.032001 PACS number(s): 13.25.Hw, 11.30.Er

I. INTRODUCTION

Decays of B mesons to two body final states containing a charmonium resonance $(J/\psi, \psi(2S), \chi_{c1})$ constitute a very sensitive laboratory for the study of electroweak transitions, as well as the dynamics of strong interactions in heavy meson systems. In particular, neutral B decays to these final states are expected to exhibit a significant CP asymmetry, the magnitude of which is clearly related to standard model parameters [1].

The tree level and leading penguin diagrams for the decay modes we consider are shown in Fig. 1. Because of the contributions of nonperturbative QCD interactions in the final state, assumptions must be made in estimating the expected branching fractions of these modes, and therefore these estimates have some degree of model dependence. A number of such estimates have appeared in the literature [2–12]. The one model-independent element common to all of these predictions is the requirement from isospin symmetry that the ratio of the charged to neutral partial widths should be unity, and that this should hold separately for each light meson accompanying the charmonium meson in the final state.

Here we report the measurement of branching fractions of B mesons to a charmonium resonance accompanied by a kaon or π^0 meson. The channels measured are listed in Table I. Here and throughout this paper for each final state mentioned its charged conjugate is also implied. We reconstruct J/ψ decays to lepton pairs l^+l^-, where l is either an electron or muon.

Our large data sample permits a measurement of these branching fractions with a precision superior to previous experiments. The simultaneous measurement of a number of final states allows us to determine ratios such as vector to pseudoscalar kaon and heavy to light charmonium states pro-

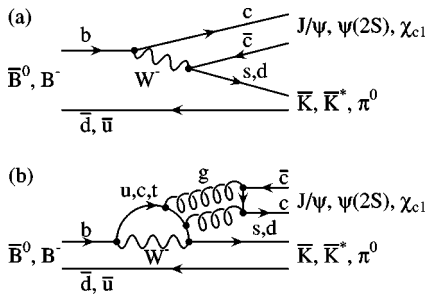

FIG. 1. Leading Feynman diagrams for the decays we consider.

*Also with Università di Perugia, Perugia, Italy.
†Also with Università della Basilicata, Potenza, Italy.

TABLE I. Branching fractions and decay modes considered in this paper. We always reconstruct the J/ψ in the l^+l^- decay mode.

Branching fraction measured	Secondary decay modes used
$B^0 \to J/\psi K^0$	$K^0 \to K^0_S$; $K^0_S \to \pi^+\pi^-$ or $\pi^0\pi^0$ $K^0 \to K^0_L$
$B^+ \to J/\psi K^+$	-
$B^0 \to J/\psi K^{*0}$	$K^{*0} \to K^+\pi^-$ or $K^0_S\pi^0$; $K^0_S \to \pi^+\pi^-$
$B^+ \to J/\psi K^{*+}$	$K^{*+} \to K^+\pi^0$ or $K^0_S\pi^+$; $K^0_S \to \pi^+\pi^-$
$B^0 \to J/\psi \pi^0$	-
$B^0 \to \psi(2S) K^0_S$	$\psi(2S) \to l^+l^-$ or $J/\psi\,\pi^+\pi^-$; $K^0_S \to \pi^+\pi^-$
$B^+ \to \psi(2S) K^+$	$\psi(2S) \to l^+l^-$ or $\psi(2S) \to J/\psi\,\pi^+\pi^-$
$B^0 \to \chi_{c1} K^0_S$	$\chi_{c1} \to J/\psi\,\gamma$; $K^0_S \to \pi^+\pi^-$
$B^+ \to \chi_{c1} K^+$	$\chi_{c1} \to J/\psi\,\gamma$
$B^0 \to \chi_{c1} K^{*0}$	$\chi_{c1} \to J/\psi\,\gamma$; $K^{*0} \to K^+\pi^-$

duction. Many systematic errors cancel when these ratios are extracted from a single data set using very similar event selection criteria, further increasing the usefulness of our results for the validation or development of phenomenological models.

Another highly relevant input for the understanding of strong interactions in B decays is the measurement of polarization in vector-vector final states, which is reported in another publication [13]. Finally, the branching fraction of $B \to J/\psi\pi^+$ is measured using a specific analysis method, reported in [14].

II. THE *BABAR* DETECTOR

The *BABAR* detector is located at the PEP-II e^+e^- storage rings operating at the Stanford Linear Accelerator Center. At PEP-II, 9.0 GeV electrons collide with 3.1 GeV positrons to produce a center-of-mass energy of 10.58 GeV, the mass of the $\Upsilon(4S)$ resonance.

The *BABAR* detector is described elsewhere [15]; here we give only a brief overview. Surrounding the interaction point is a 5 layer, double-sided silicon vertex tracker (SVT) which gives precision spatial information for all charged particles, and also measures their energy loss ($\mathrm{d}E/\mathrm{d}x$). The SVT is the primary detection device for low momentum charged particles. Outside the SVT a 40-layer drift chamber (DCH) provides measurements of the transverse momenta p_T of charged particles with respect to the beam direction. The resolution of the p_T measurement for tracks with momenta above 1 GeV/c is parametrized as

$$\frac{\sigma(p_t)}{p_T} = 0.13 p_T(\mathrm{GeV}/c)\% + 0.45\%. \qquad (1)$$

The drift chamber also measures $\mathrm{d}E/\mathrm{d}x$ with a precision of 7.5%. Beyond the outer radius of the DCH is a detector of internally reflected Cherenkov radiation (DIRC) which is used primarily for charged hadron identification. The detector consists of quartz bars in which Cherenkov light is produced as relativistic charged particles traverse the material. The light is internally reflected along the length of the bar into a water-filled stand-off box mounted on the rear of the detector. The Cherenkov rings expand in the stand-off box and are measured with an array of photomultiplier tubes mounted on its outer surface. A CsI(Tl) crystal electromagnetic calorimeter (EMC) is used to detect photons and neutral hadrons, as well as to identify electrons. The resolution of the calorimeter is parametrized as

$$\frac{\sigma(E)}{E} = \frac{2.3\%}{[E(\mathrm{GeV})]^{1/4}} \oplus 1.9\%. \qquad (2)$$

The EMC is surrounded by a superconducting solenoid that produces a 1.5-T magnetic field. The instrumented flux return (IFR) consists of multiple layers of resistive plate chambers (RPC) interleaved with the flux return iron. In addition to the planar RPC layers in the flux return, there is an additional cylindrical layer just outside of the EMC. The IFR is used in the identification of muons and neutral hadrons.

Data acquisition is triggered with a two-level system. The first level (level 1) monitors trigger information from the DCH and EMC, and generates a trigger upon detection of track or cluster candidates. The second level (level 3) retains events in which the track candidates point back to the beam interaction region (L3 DCH trigger), or EMC clusters candidates remain after the suppression of hits which have less energy than a minimum ionizing particle or are uncorrelated in time with the rest of the event (L3 EMC trigger). Over 99.9% of $B\overline{B}$ events pass either the L3 DCH or L3 EMC trigger. A fraction of all events that pass the level 1 trigger are passed through level 3 to allow monitoring of the level 3 trigger performance.

III. DATA SAMPLE

The data used in these analyses were collected between October 1999 and October 2000 and correspond to an integrated luminosity of 20.7 fb^{-1} taken on the $\Upsilon(4S)$ and 2.6 fb^{-1} taken off-resonance at an energy 0.04 GeV lower than the peak, which is below the threshold for $B\overline{B}$ production. The data set contains 22.72 ± 0.36 million $B\overline{B}$ events.

IV. COORDINATE SYSTEM AND REFERENCE FRAMES

We use a right-handed coordinate system with the z axis along the electron beam direction and y axis upwards, with origin at the nominal beam interaction point. Unless otherwise stated, kinematic quantities are calculated in the rest frame of the detector. The other reference frame we commonly use is the center of mass of the colliding electrons and positrons, which we will call the center-of-mass frame.

V. PARTICLE RECONSTRUCTION

The reconstruction of exclusive B decays begins with identifying candidates for the decay products. Charged particles are reconstructed as tracks in the SVT and/or DCH. Leptons and kaons are identified with information from the DCH, the EMC (for electrons), the IFR (for muons), and the

TABLE II. Summary of electron identification criteria. Variables used are: dE/dx, the energy loss measured in the DCH; E/p, the ratio of the EMC cluster energy to the momentum measured in the tracking spectrometer; $N_{\rm crys}$, the number of EMC crystals forming the cluster; LAT, the lateral energy distribution [16] of the EMC cluster; A_{42}, one of the Zernike moments [17] of the EMC cluster; and θ_C, the Cherenkov angle measured in the DIRC. In addition, the fraction of electrons in inclusive J/ψ events that pass each set of criteria is shown, along with the fraction of pions with momentum above 1 GeV/c that pass the selection requirements.

	DCH only	Loose	Tight	Very tight
dE/dx (measured-expected)	-2 to $+4\ \sigma_{\rm meas}$	-3 to $+7\ \sigma_{\rm meas}$	-3 to $+7\ \sigma_{\rm meas}$	-2 to $+4\ \sigma_{\rm meas}$
E/p	-	$0.65-5.0$	$0.75-1.3$	$0.89-1.2$
$N_{\rm crys}$	-	>3	>3	>3
LAT	-	-	$0.0-0.6$	$0.1-0.6$
A_{42}	-	-	-	<0.11
θ_C (measured-expected)	-	-	-	-3 to $+3\ \sigma_{\rm meas}$
Efficiency (%)	94.9	97.2	95.4	88.2
π misID (%)	21.6	4.8	1.2	0.1

DIRC (for kaons). Photons are identified based on their energy deposition in the EMC, and K_L^0 are identified from either energy deposition in the EMC or a shower in the IFR.

A. Track selection

In general, tracks used in this analysis are required to include at least 12 DCH hits to ensure that their momenta and dE/dx are well measured. In addition, tracks are required to have $p_T > 100\,{\rm MeV}/c$, and to point back to the nominal interaction point within 1.5 cm in xy and 3 cm in z. Roughly 95% of the solid angle about the interaction point in the center-of-mass frame is covered by 12 or more DCH layers.

We make exceptions to this requirement for two types of particles: pions from K_S^0, which do not originate at the nominal interaction point, and pions from $\psi(2S)\to J/\psi\pi^+\pi^-$, which frequently do not have sufficient transverse momenta to traverse 12 layers of the DCH. Any track found in the DCH or SVT is used in reconstructing these particles.

B. EMC cluster reconstruction

The energy deposited in contiguous crystals of the EMC is summed into a cluster. The distribution of energy among the crystals is used to discriminate between clusters arising from electromagnetic and hadronic showers. The variables used to describe this distribution are the lateral energy (LAT) [16] and the Zernike moments A_{mn} [17]. LAT is a measure of the radial energy profile of the cluster; the Zernike moment A_{42} measures the asymmetry of the cluster about its maximum. Electromagnetic showers have LAT peaked at about 0.25 and A_{42} close to zero, while showers from hadrons have a broader distribution in LAT and extend to larger values of A_{42}.

C. Photon candidate selection

Photons are identified as EMC clusters that do not have a spatial match with a charged track, and that have a minimum energy of 30 MeV. To reject clusters arising from noise hits, LAT is required to be less than 0.8.

D. Electron and muon identification

We derive substantial background rejection from the positive identification of electrons and muons within the sample of charged tracks. For electrons, the variables that distinguish signal from background include LAT and A_{42}, the ratio of energy measured in the EMC to momentum measured in the tracking spectrometer (E/p), dE/dx measured in the DCH, and the Cherenkov angle θ_C measured in the DIRC.

For identifying muons, the presence of an energy deposition consistent with a minimum ionizing particle in the EMC, and the details of the distribution of hits in the IFR are used. In particular, the number of interaction lengths traversed in the IFR N_λ must be consistent with expectations for a muon, both the average and variance of the number of hits per layer must be small, and the fit of a track to the hits must have low χ^2, both within the IFR ($\chi^2_{\rm IFR}$) and in the match between the IFR and central detector track ($\chi^2_{\rm match}$).

Since the optimal tradeoff between efficient selection and suppression of backgrounds varies between decay modes, there are several sets of criteria used to select leptons. These are defined in Table II for electrons and Table III for muons. In addition to these criteria, we also restrict the lepton selection to a fiducial region within which the efficiency is well known from control samples, and the material in the detector is accurately modeled in the Monte Carlo. The accepted range in polar angle θ is $0.410<\theta<2.409$ rad for electrons and $0.30<\theta<2.70$ rad for muons. This corresponds to a coverage of 84% of the solid angle in the center-of-mass frame for electrons, and 92% for muons.

To increase the efficiency of the event selection, electron candidate tracks are combined with photon candidates to recover some of the energy lost through bremsstrahlung. In addition to the photon selection criteria listed above, photons used in bremsstrahlung recovery are required to have $A_{42}<0.25$. They are also required to be within 35 mrad in θ from the track, and to have azimuthal angle ϕ intermediate between the initial track direction and the centroid of the EMC cluster arising from the track. The initial track direction is estimated by subtracting 50 mrad opposite to the bend direction from the ϕ of the fitted track measured at the ori-

TABLE III. Summary of muon identification criteria. Variables used are: $E_{\rm EMC}$, the energy deposited by the muon candidate in the EMC (this requirement is only applied for tracks within the fiducial coverage of the EMC); $N_{\rm layers}$, the number of IFR layers with hits; N_λ, the number of nuclear interaction lengths traversed; $|N_\lambda - N_\lambda({\rm exp})|$, the difference between the number of nuclear interaction lengths traversed and the expectation for a muon of the measured momentum; $\langle N_{\rm hit}\rangle$, the average number of hits per IFR layer; ${\rm RMS}_{\rm hit}$, the RMS of the distribution of the number of hits on each layer; $f_{\rm hit}$, the fraction of layers between the innermost and outermost hit layers that also have hits (this requirement is only applied in the region covered partly or entirely by the endcap IFR system, $0.3<\theta<1.0$); $\chi^2_{\rm IFR}$, the χ^2 of the track in the IFR; and $\chi^2_{\rm match}$, the χ^2 of the match between the IFR track and the track from the central detector. In addition, the fraction of muons in inclusive J/ψ events that pass each set of criteria is shown, along with the fraction of pions with momentum above 1 GeV/c that pass the selection requirements.

	MIP	Very Loose	Loose	Tight	Very tight
$E_{\rm EMC}$ (GeV)	<0.5	<0.5	<0.5	$0.05-0.4$	$0.05-0.4$
$N_{\rm layers}$	-	>1	>1	>1	>1
N_λ	-	>2	>2	>2.2	>2.2
$\lvert N_\lambda - N_\lambda({\rm exp})\rvert$	-	<2.5	<2.0	<1	<0.8
$\langle N_{\rm hit}\rangle$	-	<10	<10	<8	<8
${\rm RMS}_{\rm hit}$	-	<6	<6	<4	<4
$f_{\rm hit}$	-	>0.1	>0.2	>0.3	>0.34
$\chi^2_{\rm IFR}$	-	-	$<4\times N_{\rm layers}$	$<3\times N_{\rm layers}$	$<3\times N_{\rm layers}$
$\chi^2_{\rm match}$	-	-	$<7\times N_{\rm layers}$	$<5\times N_{\rm layers}$	$<5\times N_{\rm layers}$
Efficiency (%)	99.6	92.2	86.2	70.3	67.0
π misID (%)	57.9	14.5	7.0	2.4	2.1

gin. The procedure increases the efficiency for reconstructing charmonium decays to e^+e^- by about 30%.

E. K_L^0 candidate selection

We identify neutral hadrons through the presence of an energy deposition in the EMC or a cluster in the IFR. Neutral hadrons must be spatially separated from all tracks in the event. In reconstructing the decay $B^0\to J/\psi K_L^0$ neutral hadrons are taken as K_L^0 candidates, with requirements specifically tailored for this mode.

Only the measured direction of the neutral hadron is used for K_L^0 reconstruction, as its energy is poorly measured. The direction of the K_L^0 candidate is defined by the line joining the vertex of the J/ψ candidate and the centroid of the EMC or IFR cluster.

For a K_L^0 to reach the IFR it must traverse the EMC material, which amounts to approximately one nuclear interaction length. As a consequence, half of the K_L^0 mesons undergo detectable interactions in the EMC. We consider EMC clusters with energy in the 0.2–2.0 GeV range. Most clusters arising from K_L^0 interactions have energy below the upper bound; below the lower bound the contamination from noise becomes significant. All such EMC clusters which are spatially separated from a track are considered as K_L^0 candidates, except those that combined with another neutral cluster give an invariant mass compatible with a π^0.

About 60% of K_L^0 mesons from $B^0\to J/\psi K_L^0$ leave a detectable signal in the IFR. We select K_L^0 candidates in the IFR starting with clusters of hits not spatially matched to a track. IFR clusters with hits only in the outer layers of the forward endcap are rejected to reduce the contribution from beam backgrounds.

VI. EVENT SELECTION AND *B* MESON COUNTING

A determination of B meson branching fractions depends upon an accurate measurement of the number of B mesons in the data sample. We find the number of $B\overline{B}$ pairs by comparing the rate of multihadron events in data taken on the $\Upsilon(4S)$ resonance to that in data taken off-resonance. The $B\overline{B}$ purity of the sample is enhanced by requiring the events to pass the following selection criteria, in which all tracks (including those that do not satisfy our usual selection requirements) in the fiducial region $0.410<\theta<2.54$ rad and all neutral clusters with energy greater than 30 MeV in the region $0.410<\theta<2.409$ rad are considered:

The event must satisfy either the L3 DCH or L3 EMC trigger.

There must be at least three tracks that satisfy the standard selection requirements in the fiducial region.

The ratio of the second to the zeroth Fox-Wolfram moment [18] must be less than 0.5.

The event vertex is calculated by an iterative procedure that begins by considering every track in the event, and then discards those that contribute a large χ^2 to the fit (these are presumed to arise from the decay of long-lived particles) until the vertex fit is stable. This vertex must be within 0.5 cm of the beam spot center in xy and within 6 cm in z. The beam spot has a rms width of about 120 μm in x, 5.9 μm in y, and 0.9 cm in z. The point of closest approach of a high-momentum track to the beam spot is measured with a resolution of 23 μm in x and y, and 29 μm in z, as determined with dimuon events.

TABLE IV. Summary of observed invariant mass or mass difference Δm widths for all intermediate mesons considered in this paper. For most mesons the width is dominated by experimental resolution, and the value reported in the table is the width σ from a Gaussian fit to the data. For the K^* modes the natural width of the resonance dominates, and the value reported is the full width of a Breit-Wigner fit to the data. The width for J/ψ and $\psi(2S)$ decaying to e^+e^- is greater than that for $\mu^+\mu^-$ due to the energy lost through bremsstrahlung.

Quantity	Decay mode	Width (MeV/c^2)
J/ψ mass	e^+e^-	17 ± 2
	$\mu^+\mu^-$	13 ± 1
$\psi(2S)$ mass	e^+e^-	29 ± 6
	$\mu^+\mu^-$	21 ± 3
$\Delta m(\psi(2S)-J/\psi)$	$\psi(2S)\to J/\psi\,\pi^+\pi^-$; $J/\psi\to l^+l^-$	7 ± 1
$\Delta m(\chi_{c1}-J/\psi)$	$J/\psi\to l^+l^-$	14 ± 1
K^0_S mass	$\pi^+\pi^-$	3.5 ± 0.2
	$\pi^0\pi^0$	15 ± 2
K^{*0} mass	$K^+\pi^-$ and $K^0_S\pi^0$	60 ± 7
K^{*+} mass	$K^0_S\pi^+$ and $K^+\pi^0$	50 ± 10

The total energy of charged and neutral particles is required to be greater than 4.5 GeV.

These requirements are $95.4\pm1.4\%$ efficient for $B\overline{B}$ events, as estimated from a Monte Carlo simulation. All events used in the branching fraction analyses are required to pass this selection.

VII. MESON CANDIDATE SELECTION

The next step in the analysis is to combine sets of tracks and/or neutral clusters to form candidates for the initial or intermediate mesons in the decay. Our general strategy when forming these candidates is to assign the expected masses to tracks and neutral clusters, and to apply a vertex constraint before computing the invariant mass. In rare instances (less than 1% of all meson candidates) the vertex fit does not converge. The sum of the track and/or cluster four-vectors is used to compute the invariant mass for such candidates. If one or more decay products from a given particle are themselves intermediate states, we constrain them to their known masses. At each step in the decay chain, we require that mesons have masses consistent with their assumed particle type. The mass resolutions observed for all of the intermediate mesons considered in this paper are listed in Table IV.

We choose meson selection criteria to maximize the expected precision of our branching fraction measurements. Therefore we use well-understood quantities in our selection, which lead to a smaller systematic uncertainty. We set the selection values to maximize the ratio $S/\sqrt{S+B}$ where S and B are the expected number of signal and background events respectively, as estimated from Monte Carlo calculations. If a given mode has been previously observed, S is estimated using the known branching fraction. Otherwise, selection values similar to those in previously-observed modes are taken as a starting point, and then modified to reduce background (as measured in the kinematic sidebands) or increase signal efficiency (as measured using Monte Carlo simulated signal events). In most cases, we find that $S/\sqrt{S+B}$ does not change significantly when selection values are varied near their optima. This allows us to choose standard selection values across most final states.

A. Charmonium meson candidate selection

1. J/ψ selection

J/ψ candidates are required to have an invariant mass in the range $2.95<M_{J/\psi}<3.14\,\mathrm{GeV}/c^2$ and $3.06<M_{J/\psi}<3.14\,\mathrm{GeV}/c^2$ for $J/\psi\to e^+e^-$ and $J/\psi\to\mu^+\mu^-$ decays, respectively. Unless otherwise stated, for $J/\psi\to e^+e^-$ decays, one track is required to pass the tight electron selection and the other the loose selection. Tracks not associated to an EMC cluster that pass the DCH-only selection are also accepted. For $J/\psi\to\mu^+\mu^-$ decays, we require one track to pass the loose selection and the other to pass the MIP selection.

The mass distribution for J/ψ candidates in the data is shown in Fig. 2.

2. $\psi(2S)$ selection

$\psi(2S)\to\mu^+\mu^-$ candidates are required to have a mass within 50 MeV/c^2 of the known $\psi(2S)$ value of 3.69 GeV/c^2 [19]. For $\psi(2S)\to e^+e^-$ candidates the lower bound is relaxed to 250 MeV/c^2 below the known value. For decays of the $\psi(2S)$ to $J/\psi\,\pi^+\pi^-$, the difference in mass between the $\psi(2S)$ and J/ψ candidates is required to be within $15\,\mathrm{MeV}/c^2$ of the expected value, and the $\pi^+\pi^-$ invariant mass $m_{\pi^+\pi^-}$ is required to be between 0.4 and $0.6\,\mathrm{GeV}/c^2$. The latter requirement takes advantage of the fact that $m_{\pi^+\pi^-}$ is most often in the upper portion of the kinematically allowed range [20]. All $\psi(2S)$ candidates are required to have a momentum in the center-of-mass frame between 1.0 and 1.6 GeV/c, consistent with $B\to\psi(2S)K$ decays.

We have used the same lepton identification requirements as for the J/ψ reconstruction. These are applied either to the leptons from $\psi(2S)\to l^+l^-$ decays, or to the leptons from the J/ψ in $\psi(2S)\to J/\psi\,\pi^+\pi^-$ decays.

The mass and mass difference distributions for $\psi(2S)$ candidates in the data are shown in Fig. 3. For Figs. 3, 4, and 6 a background subtraction is performed using the observed distribution of candidates in the ΔE sidebands (see Sec. VII C).

3. χ_{c1} selection

In reconstructing $\chi_{c1}\to J/\psi\gamma$, J/ψ and photon candidates are selected as described above. The muon identification requirements are subsequently tightened by demanding that one lepton from the J/ψ pass the loose selection and the other the very loose selection (rather than the MIP selection).

In addition, the photon cluster is required to satisfy $E>150\,\mathrm{MeV}$ and $A_{42}<0.15$ and to have a centroid in the an-

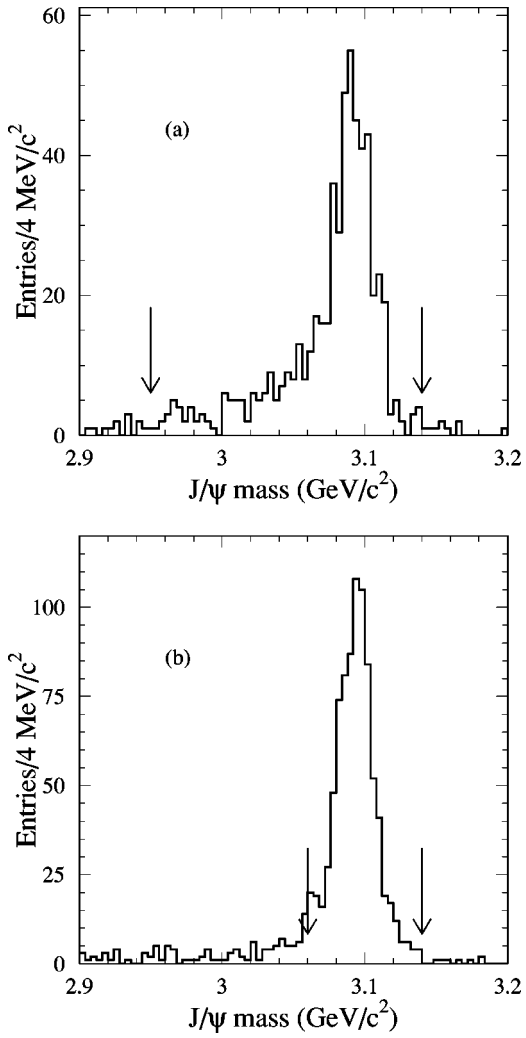

FIG. 2. Invariant mass distribution for (a) $J/\psi \to e^+e^-$ and (b) $J/\psi \to \mu^+\mu^-$ candidates observed in $B^0 \to J/\psi K_S^0$ and $B^+ \to J/\psi K^+$ candidates passing the exclusive branching fraction selection. The mass interval used to select J/ψ candidates for B reconstruction is indicated by the arrows.

gular range $0.41 < \theta < 2.409$, excluding the forward direction due to the increased material (from electronics, cables, and final-focusing magnets) in that region.

We require the mass difference between the reconstructed χ_{c1} and J/ψ candidates to satisfy $0.35 < M_{\gamma J/\psi} - M_{J/\psi} < 0.45\,\mathrm{GeV}/c^2$.

The mass difference distribution for χ_{c1} candidates in the data is shown in Fig. 4.

B. Light meson candidate selection

1. $\pi^0 \to \gamma\gamma$ selection

We reconstruct π^0 candidates as pairs of photons. Individual photons separated by distances of 10 cm or more in the EMC are reconstructed as distinct clusters. Photons from π^0's with energies above 2 GeV can have less separation, in which case the two photons are reconstructed as a single cluster. We refer to these as ''merged'' π^0's. They are distinguished from single photons based on their shower shape.

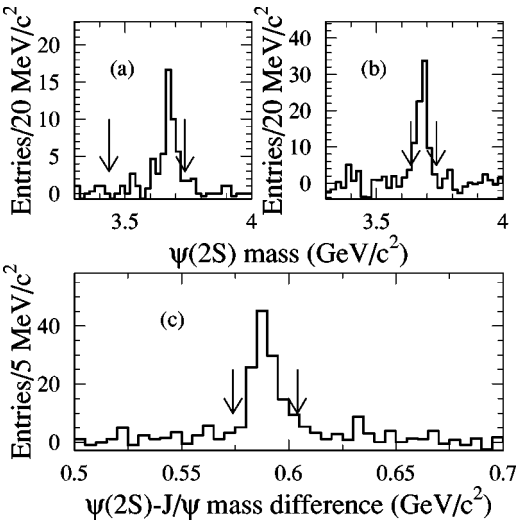

FIG. 3. Background-subtracted $\psi(2S)$ candidate mass and mass difference distributions observed in $B^0 \to \psi(2S)K_S^0$ and $B^+ \to \psi(2S)K^+$ candidates passing the exclusive branching fraction selection, for (a) $\psi(2S) \to e^+e^-$, (b) $\psi(2S) \to \mu^+\mu^-$, and (c) the $\psi(2S)$-J/ψ mass difference distribution for $\psi(2S) \to J/\psi\ \pi^+\pi^-$. The intervals used to select $\psi(2S)$ candidates for B reconstruction are indicated by the arrows.

2. $K_S^0 \to \pi^+\pi^-$ selection

We construct K_S^0 candidates from all pairs of oppositely charged tracks, and retain those that have invariant mass between 489 and 507 MeV/c^2 after applying a vertex constraint. To further reject background we exploit the flight length of the K_S^0 by demanding that the K_S^0 vertex be more than 1 mm (in three dimensions) from the J/ψ, $\psi(2S)$, or χ_{c1} vertex.

The mass distribution for $K_S^0 \to \pi^+\pi^-$ candidates in the data is shown in Fig. 5.

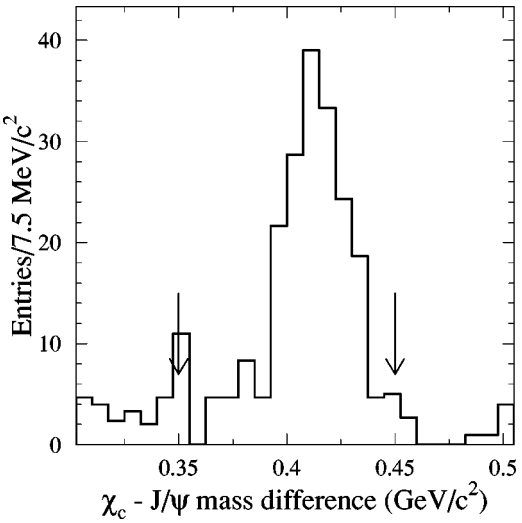

FIG. 4. Background-subtracted χ_{c1}-J/ψ candidate mass difference distribution observed in $B^0 \to \chi_{c1}K_S^0$ and $B^+ \to \chi_{c1}K^+$ candidates passing the exclusive branching fraction selection. The mass difference interval used to select χ_{c1} candidates for B reconstruction is indicated by the arrows.

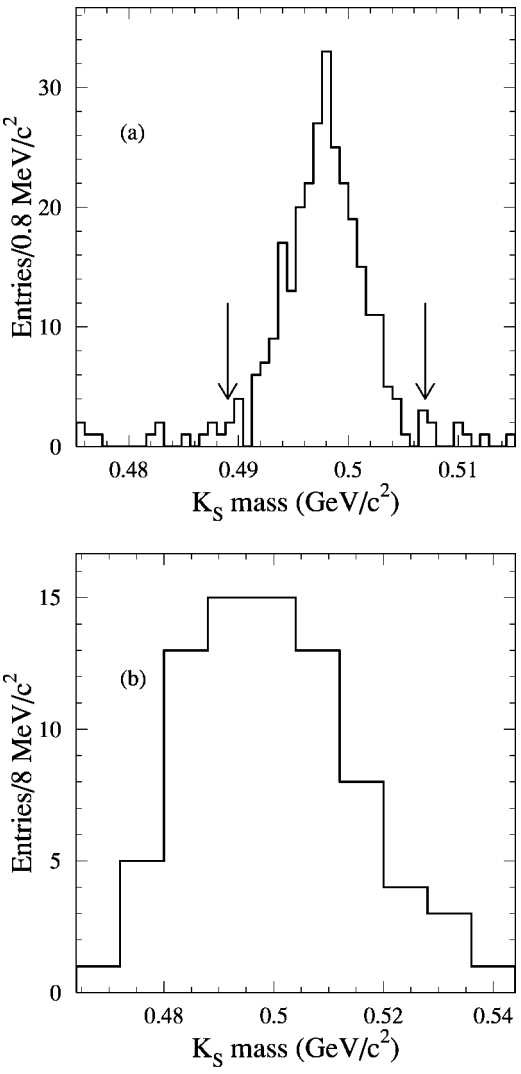

FIG. 5. K_S^0 candidate mass distribution observed in $B^0 \to J/\psi K_S^0$ candidates passing the exclusive branching fraction selection, for (a) $K_S^0 \to \pi^+\pi^-$ and (b) $K_S^0 \to \pi^0\pi^0$. The mass intervals used to select $K_S^0 \to \pi^+\pi^-$ candidates for B reconstruction is indicated by the arrows in (a); the full range of (b) is used in selecting $K_S^0 \to \pi^0\pi^0$ candidates.

3. $K_S^0 \to \pi^0\pi^0$ selection

The $K_S^0 \to \pi^0\pi^0 \to 4\gamma$ decay chain is reconstructed from photon combinations satisfying $E_\gamma > 30\,\mathrm{MeV}$, $E_{\pi^0} > 200\,\mathrm{MeV}$ and $E_{K_S^0} > 800\,\mathrm{MeV}$, with $110 \leqslant m_{\pi^0} \leqslant 155\,\mathrm{MeV}/c^2$ and $300 \leqslant m_{K_S^0} \leqslant 800\,\mathrm{MeV}/c^2$. We perform a mass-constrained fit to each photon pair with the known π^0 mass. This fit is repeated assuming different decay points along the K_S^0 flight path, as defined by the J/ψ vertex and the initial K_S^0 momentum vector direction. The point where the product of the fit χ^2 probabilities for the two π^0's is maximal is defined as the K_S^0 decay vertex. K_S^0 candidates with flight length in the range from -10 to $+40$ cm are retained.

We consider merged π^0 candidates with energy above 1 GeV. If an EMC cluster candidate is identified as a merged π^0 but can also be paired with another photon to form a π^0 candidate, we use the latter interpretation. Merged π^0's represent less than 10% of all π^0's used in this analysis.

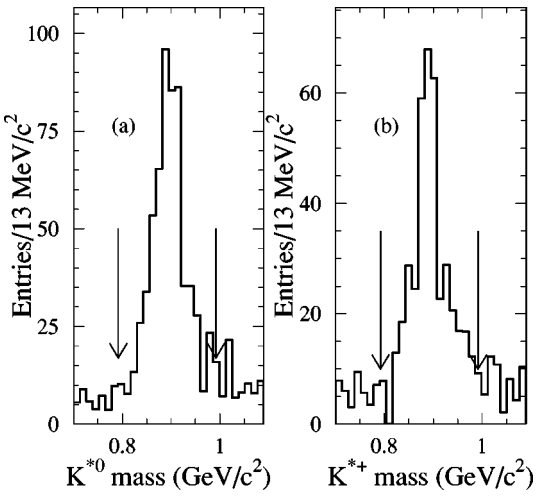

FIG. 6. Background-subtracted (a) K^{*0} and (b) K^{*+} candidate mass distributions observed in $B^0 \to J/\psi K^{*0}$ and $B^+ \to J/\psi K^{*+}$ candidates passing the exclusive branching fraction selection. The mass interval used to select K^* candidates for B reconstruction is indicated by the arrows.

The invariant mass of the K_S^0 candidate at the optimal vertex point is required to lie in the range 470 to $550\,\mathrm{MeV}/c^2$.

The mass distribution for $K_S^0 \to \pi^0\pi^0$ candidates in the data is shown in Fig. 5.

4. K^{*0} and K^{*+} reconstruction

We reconstruct the K^{*0} through its decays to $K^+\pi^-$ and $K_S^0\pi^0$ and the K^{*+} through its decays to $K_S^0\pi^+$ and $K^+\pi^0$, where the K_S^0 is reconstructed in the $\pi^+\pi^-$ mode.

π^0's are reconstructed from isolated photons and required to have an invariant mass between 106 and $153\,\mathrm{MeV}/c^2$. If there is a K_S^0 in the final state we require that the angle in the xy plane between the K_S^0 momentum vector and the line joining the J/ψ and K_S^0 vertices be less than 200 mrad and that the K_S^0 vertex fit converge.

In addition, for channels containing a π^0 in the final state, we demand that the cosine of the angle θ_K, measured in the K^* rest frame, between the kaon momentum and the K^* direction as measured in the B frame be less than 0.95.

All candidate K^*'s are required to be within $100\,\mathrm{MeV}/c^2$ of the known K^{*0} or K^{*+} mass [19].

The mass distribution for K^* candidates in the data is shown in Fig. 6.

C. B meson candidate selection

B mesons are reconstructed by combining charmonium meson candidates with light meson candidates. Both the charmonium and light meson candidates are constrained to their known masses, with the exception of K^* candidates, for which the natural width dominates the experimental resolution. Two kinematic variables are used to isolate the B meson signal for all modes except $B^0 \to J/\psi K_L^0$. One is the difference between the reconstructed energy of the B candidate

TABLE V. Definition of the signal region in $|\Delta E|$ and $m_{\rm ES}$ for each mode used in this analysis. The $m_{\rm ES}$ signal region is given in terms of $|m_{\rm ES}-m_B|$, where m_B is 5279 MeV/c^2.

B decay mode	Light meson decay mode	Charmonium meson decay mode	$\|\Delta E\|$ (MeV)	$\|m_{\rm ES}-m_B\|$ (MeV/c^2)
$B^0\to J/\psi K_S^0$	$\pi^+\pi^-$	e^+e^-	34.5	8.1
		$\mu^+\mu^-$	29.0	7.2
	$\pi^0\pi^0$	e^+e^-	100.0	8.0
		$\mu^+\mu^-$	100.0	10.0
$B^0\to J/\psi K_L^0$	-	e^+e^- & $\mu^+\mu^-$	10.0	-
$B^+\to J/\psi K^+$	-	e^+e^-	38.4	7.5
		$\mu^+\mu^-$	30.3	6.9
$B^0\to J/\psi K^{*0}$	$K^+\pi^-$	e^+e^-	30.9	9.3
		$\mu^+\mu^-$	23.7	8.1
	$K_S^0\pi^0$	e^+e^-	48.6	12.0
		$\mu^+\mu^-$	45.6	11.4
$B^-\to J/\psi K^{*+}$	$K_S^0\pi^-$	e^+e^-	62.7	7.2
		$\mu^+\mu^-$	20.4	9.9
	$K^+\pi^0$	e^+e^-	85.2	11.4
		$\mu^+\mu^-$	50.1	10.2
$B^0\to J/\psi\pi^0$	$\gamma\gamma$	e^+e^- & $\mu^+\mu^-$	112.0	9.0
$B^0\to\psi(2S)K_S^0$	$\pi^+\pi^-$	e^+e^- & $e^+e^-\,\pi^+\pi^-$	28.0	9.0
		$\mu^+\mu^-$ & $\mu^+\mu^-\,\pi^+\pi^-$	26.0	9.0
$B^+\to\psi(2S)K^+$	$\pi^+\pi^-$	e^+e^- & $e^+e^-\,\pi^+\pi^-$	28.0	9.0
		$\mu^+\mu^-$ & $\mu^+\mu^-\,\pi^+\pi^-$	26.0	9.0
$B^0\to\chi_{c1}K_S^0$	$\pi^+\pi^-$	$e^+e^-\gamma$	30.9	6.9
		$\mu^+\mu^-\gamma$	21.4	6.9
$B^+\to\chi_{c1}K^+$	$\pi^+\pi^-$	$e^+e^-\gamma$	33.9	11.7
		$\mu^+\mu^-\gamma$	27.9	6.6
$B^0\to\chi_{c1}K^{*0}$	$K^+\pi^-$	$e^+e^-\gamma$	30.0	9.0
		$\mu^+\mu^-\gamma$	30.0	9.0

and the beam energy in the center-of-mass frame ΔE. The other is the beam energy substituted mass $m_{\rm ES}$, defined as

$$m_{\rm ES}=\sqrt{E^{*2}_{\rm beam}-p^{*2}_B} \tag{3}$$

where p_B^* is the momentum of the reconstructed B and $E^*_{\rm beam}$ is the beam energy, both in the center-of-mass frame. The small variations of $E^*_{\rm beam}$ over the duration of the run are taken into account when calculating $m_{\rm ES}$. Signal events will have ΔE close to 0 and $m_{\rm ES}$ close to the B meson mass, 5.279 GeV/c^2.

We limit all our two dimensional plots in these variables to the ''signal neighborhood,'' defined by $|\Delta E|<\Delta E_{\rm max}$ and $5.2<m_{\rm ES}<5.3\,{\rm GeV}/c^2$. For most channels, $\Delta E_{\rm max}$ is 120 MeV, but for the $B^0\to J/\psi K_S^0(K_S^0\to\pi^0\pi^0)$ and $B^0\to J/\psi\pi^0$ channels, which have larger ΔE resolution, it is increased to 150 and 400 MeV, respectively. We define the signal region by fitting the observed distribution of events in the signal neighborhood in $m_{\rm ES}$ and ΔE separately. In the fit, the signal component is modelled by a Gaussian, and the background component is modelled by an empirical phase-space distribution [21] (henceforth referred to as the ARGUS distribution) when fitting the $m_{\rm ES}$ distribution, or a polynomial when fitting the ΔE distribution. The ARGUS distribution is

$$A(m_{\rm ES};m_0,c)\propto m_{\rm ES}\sqrt{1-(m_{\rm ES}/m_0)^2}\times\exp(c[1-(m_{\rm ES}/m_0)^2]), \tag{4}$$

where m_0 is set to a typical beam energy and c is a fitted parameter.

The widths of the fitted Gaussian provide a measurement of the resolution in ΔE and $m_{\rm ES}$, and the signal region is defined as $\pm3\sigma$ about the nominal value in each variable. The resolution in $m_{\rm ES}$ is typically 3 MeV/c^2, and that in ΔE is typically 10 MeV for channels with no neutral particles in the final state and 30 MeV otherwise. The signal region for each mode is given in Table V.

A somewhat different procedure is required for reconstructing $B^0\to J/\psi K_L^0$, since the K_L^0 energy is not measured. Either the B mass or energy must be constrained, leaving only one independent variable. We choose to fix the B mass to its known value [19] and plot the signal in the quantity $\Delta E_{K_L^0}\equiv E^*_{J/\psi}+E^*_{K_L^0}-E^*_{\rm beam}$, where $E^*_{J/\psi}$ is the energy of the mass-constrained J/ψ, and $E^*_{K_L^0}$ is the energy of the K_L^0 as determined using the B mass constraint, both in the center-of-mass frame. $\Delta E_{K_L^0}$ is a measure of the same quantity as ΔE; we use the different notation to reflect the fact that the

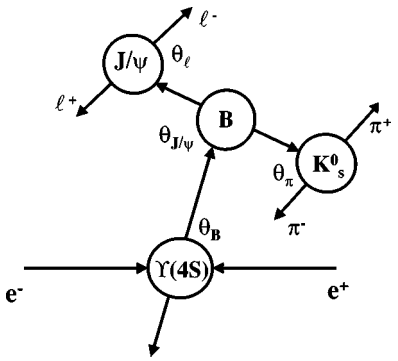

FIG. 7. Helicity angles for the decay $\Upsilon(4S)\to B\bar{B}\to J/\psi$ $(e^+e^-$ or $\mu^+\mu^-)+K_S^0$.

B mass constraint is used only in this channel. For signal, $\Delta E_{K_L^0}$ is expected to peak at zero with a resolution of approximately 3.5 MeV. The signal region is defined as $|\Delta E_{K_L^0}|<10$ MeV.

1. Helicity and thrust angle definitions

We use the helicity angles θ_B and θ_l to help distinguish signal from background. θ_B is the angle in the center-of-mass frame between the electron beam and B candidate directions, and θ_l is the angle in the charmonium meson rest frame between the l^- and light meson candidate directions. Figure 7 gives a schematic representation of these angles for the decay $B^0\to J/\psi K_S^0$.

The angle θ_B has a $\sin^2\theta_B$ distribution for $\Upsilon(4S)$ meson decays. If X is a pseudoscalar (K^0,K^+,π^0) then the charmonium meson must be longitudinally polarized, and the resulting θ_l distribution is proportional to $\sin^2\theta_l$. If X is a vector (K^*) the decay angular distribution depends on more than one helicity amplitude. In this case the lepton angular distributions are not known *a priori* and must be experimentally determined.

The B candidates formed from light quark backgrounds will generally follow a $1+\cos^2\theta_B$ angular distribution. The θ_l helicity angle is especially useful in rejecting background since the distribution of $\cos\theta_l$ is peaked at ±1 for background and at zero for signal for modes where X is a pseudoscalar. As an example, the distribution of $\cos\theta_l$ observed in data for $B^0\to J/\psi K_S^0$ and $B^+\to J/\psi K^+$ candidates is shown in Fig. 8.

For modes where the charmonium meson decays to more than two bodies, and θ_l is therefore undefined, we suppress backgrounds using the thrust angle θ_T, defined as the angle between the thrust axis of the reconstructed B and that of the rest of the event in the center-of-mass frame. We use the conventional definition of the thrust axis for a collection of particles as the direction about which the transverse momenta of the particles is minimized. In $B\bar{B}$ events $\cos\theta_T$ is uniformly distributed, whereas in continuum background events θ_T tends to peak at π radians due to the two-jet nature of these events. Hence θ_T can be used to discriminate against background in modes where the helicity angle is not applicable.

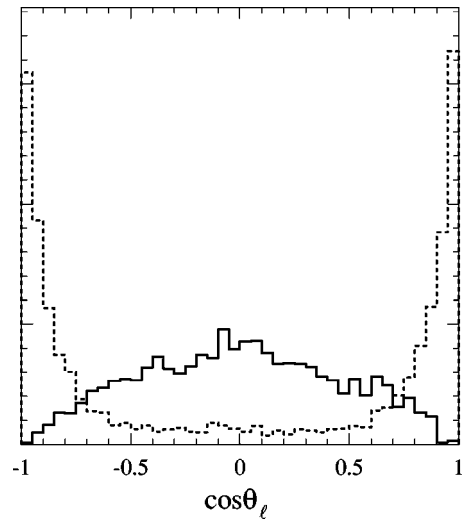

FIG. 8. Distributions of $\cos\theta_l$ observed in $B^0\to J/\psi K_S^0$ and $B^+\to J/\psi K^+$ candidates. The dashed histogram shows candidates in the ΔE sideband. The solid histogram shows the distribution in the ΔE-$m_{\rm ES}$ signal region, after subtracting the distribution observed in the sideband scaled by the ratio of signal to sideband areas. The normalization of both histograms has been set to unity.

The helicity and thrust angle values used to select candidates are listed in the appropriate exclusive reconstruction and selection subsections in this paper.

2. Multiple candidates

We only allow one exclusive candidate per event in a given decay mode. In the cases where we have multiple candidates (less than 10% of all events with a candidate for most modes, but up to 30% for the K^* modes which have significant crossfeed among decay channels), the candidate with the lowest $|\Delta E|$ is taken over all others. The only exception is in the $B^0\to J/\psi K_L^0$ selection, where we choose the candidate with the largest K_L^0 energy as measured by the EMC. If none of the candidate K_L^0 mesons have EMC information, we choose the candidate that has the largest number of layers with hits in the IFR. These criteria are chosen because background K_L^0 candidates often arise from low-energy photons in the EMC or electronics noise or hadronic split-offs in the IFR.

3. $B^0\to J/\psi K_S^0(\pi^+\pi^-)$

All combinations of J/ψ and $K_S^0\to\pi^+\pi^-$ candidates are used to form B candidates. We require the absolute value of $\cos\theta_l$ to be less than 0.8 and 0.9 for $J/\psi\to e^+e^-$ and $J/\psi\to\mu^+\mu^-$ events, respectively. The distribution of the selected candidates in ΔE and $m_{\rm ES}$ is shown in Fig. 9(a).

4. $B^0\to J/\psi K_S^0(\pi^0\pi^0)$

All combinations of J/ψ and $K_S^0\to\pi^0\pi^0$ candidates are considered. For $J/\psi\to e^+e^-$ candidates, one track is required to pass the tight or DCH-only selection, and no particle identification requirement is placed on the second track. The mass-constrained J/ψ vertex is assumed to be the pro-

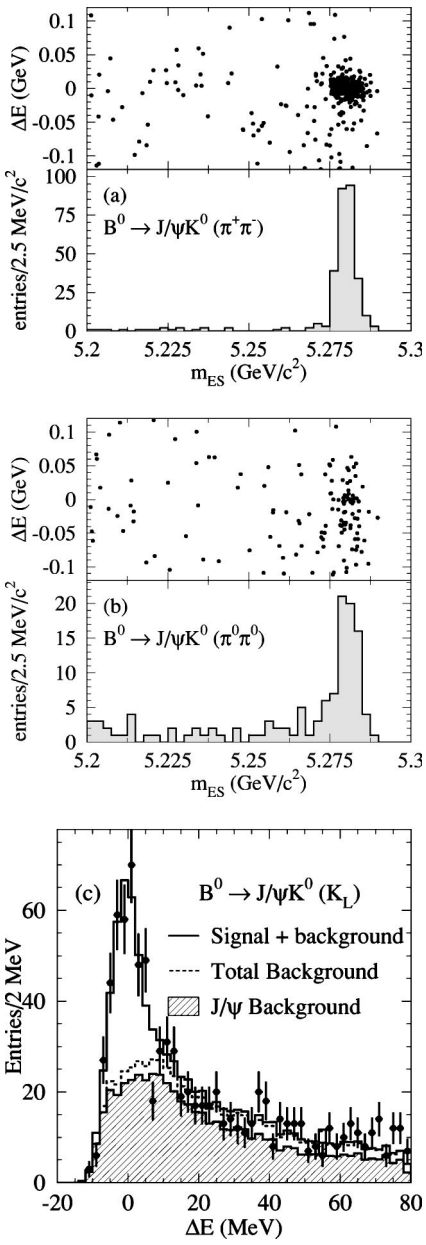

FIG. 9. Signals for $B^0 \to J/\psi K_S^0$ [(a) $K_S^0 \to \pi^+\pi^-$ and (b) $K_S^0 \to \pi^0\pi^0$] and (c) $B^0 \to J/\psi K_L^0$. In (a) and (b) the upper plots show the distribution of events in the ΔE-$m_{\rm ES}$ plane, and the lower plots show the distribution in $m_{\rm ES}$ of events in the signal region in ΔE. In (c) the points are the data, the dashed line shows the Monte Carlo simulated distribution of background events which include a real J/ψ, the hatched area shows the model for the total background, where the non-J/ψ component is taken from the J/ψ sidebands in data, and the solid line shows the sum of the background and signal Monte Carlo models.

duction point of the K_S^0. We require that the absolute value of $\cos\theta_l$ be less than 0.7 and 0.8 for $J/\psi \to e^+e^-$ and $J/\psi \to \mu^+\mu^-$ events, respectively. The distribution of the selected candidates in ΔE and $m_{\rm ES}$ is shown in Fig. 9(b).

5. $B^0 \to J/\psi K_L^0$

Since most of the background in this mode arises from B decays that include charmonium mesons, we reject events if they contain a candidate for $B^0 \to J/\psi K_S^0$, $B^+ \to J/\psi K^+$, $B^0 \to J/\psi K^{*0}$, or $B^+ \to J/\psi K^{*+}$. The decay modes used to reconstruct these candidates are the same as those used in the branching fraction analysis for each mode, but the selection criteria are loosened.

Within the remaining events, we select J/ψ candidates using a procedure that differs slightly from the standard selection. A vertex constraint is applied, and only candidates for which the fit converges are retained. In addition the momentum of the J/ψ in the center of mass frame is required to be between 1.4 and 2.0 GeV/c, consistent with $B^0 \to J/\psi K_L^0$ decays. In the e^+e^- mode, one electron candidate is required to pass the very tight selection and the other the loose selection, and the J/ψ mass is required to be between 3.00 and 3.13 GeV/c^2. For the $\mu^+\mu^-$ mode one muon candidate must pass the tight selection and the other the loose selection, and the J/ψ mass is required to be between 3.06 and 3.13 GeV/c^2.

We consider all pairs of K_L^0 and J/ψ candidates, as described above, as candidates for $B \to \psi K_L^0$ decays. We then construct the quantity $\Delta E_{K_L^0}$ described previously.

For candidates containing a K_L^0 that is identified in the EMC, we require that the transverse missing momentum be consistent with the momentum of the K_L^0 candidate calculated from the B mass constraint. We compute the missing momentum from all tracks and EMC clusters, omitting the K_L^0 candidate cluster. This quantity is then projected along the direction of the K_L^0 candidate in the plane transverse to the beam. Studies of $B^0 \to J/\psi K_L^0$ events in the simulation imply that the event missing momentum should be equal to the calculated momentum of the K_L^0, with a resolution of 0.30 GeV/c. Therefore, we select events where the total missing momentum is not less than 0.65 GeV/c below the calculated K_L^0 momentum. The missing momentum requirement is not applied when the K_L^0 candidate is identified in the IFR, since the background is much lower in this sample.

For all events, we use the angles θ_B and θ_l to suppress background. We require that $|\cos\theta_B|$ and $|\cos\theta_l|$ be less than 0.9. To further reduce background, we also demand that $|\cos\theta_B| + |\cos\theta_l|$ be less than 1.3.

The distribution of the selected candidates in $\Delta E_{K_L^0}$ is shown in Fig. 9(c).

6. $B^+ \to J/\psi K^+$

Every combination of a J/ψ candidate and a track is considered. We require $|\cos\theta_l|$ to be less than 0.8 and 0.9 for $J/\psi \to e^+e^-$ and $J/\psi \to \mu^+\mu^-$ events, respectively. The distribution of the selected candidates in ΔE and $m_{\rm ES}$ is shown in Fig. 10(a).

7. $B^0 \to J/\psi \pi^0$

For $J/\psi \to \mu^+\mu^-$ the standard selection is tightened by requiring that one charged track satisfy the very tight criteria and the other the loose criteria. Only π^0's formed from isolated photon pairs with mass between 120 and 150 MeV/c^2 are considered.

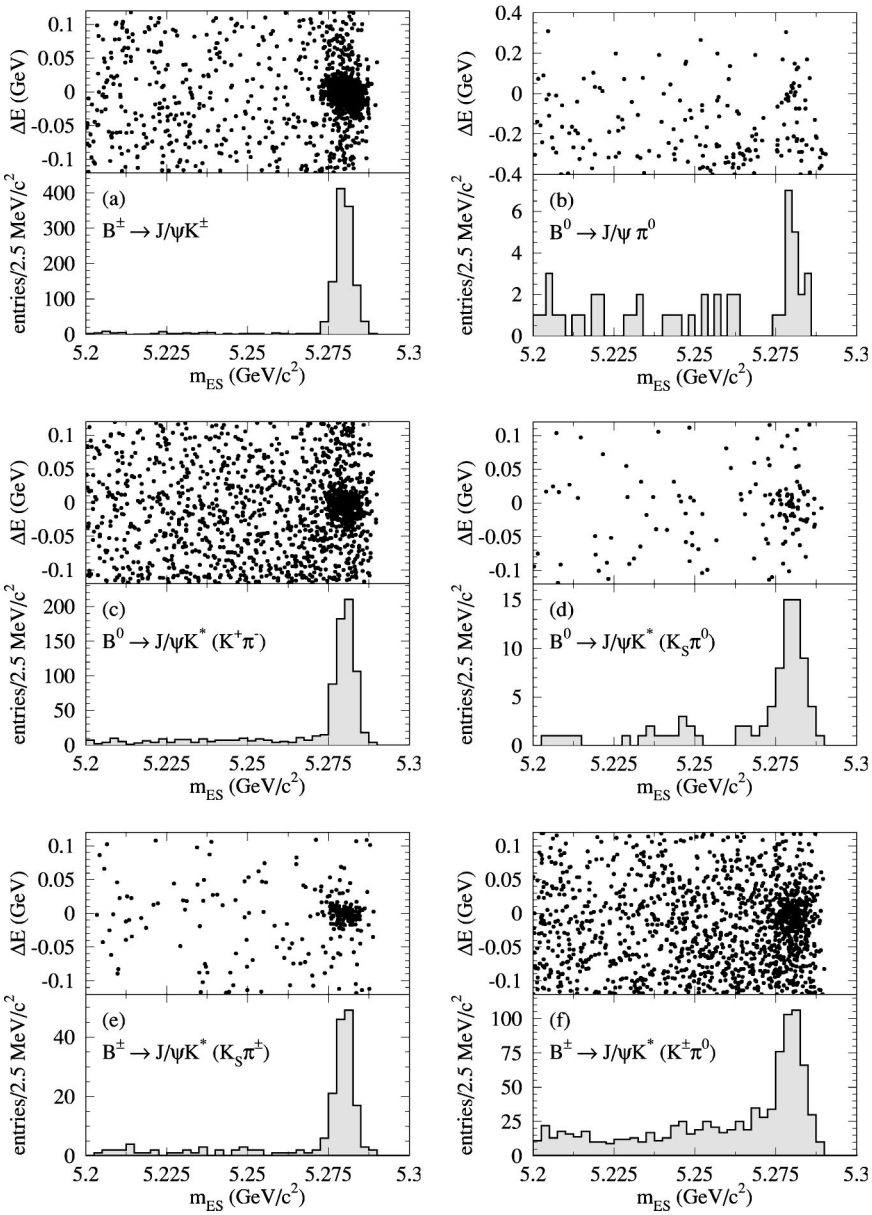

FIG. 10. Signal for (a) $B^+ \to J/\psi K^+$, (b) $B^0 \to J/\psi \pi^0$, (c), (d) $B^0 \to J/\psi K^{*0}$, and (e), (f) $B^+ \to J/\psi K^{*+}$. The upper plots show the distribution of events in the ΔE-$m_{\rm ES}$ plane, and the lower plots show the distribution in $m_{\rm ES}$ of events in the signal region in ΔE.

The absolute value of $\cos\theta_T$ is required to be less than 0.95. Since continuum background events are slightly correlated in θ_T and θ_l we also demand that $|\cos\theta_T|+|\cos\theta_l|$ be less than 1.8. The distribution of the selected candidates in ΔE and $m_{\rm ES}$ is shown in Fig. 10(b). Monte Carlo simulation shows that the cluster of events near the $m_{\rm ES}$ signal value but with low ΔE arises from inclusive charmonium background events, where $B^0 \to J/\psi K^0_S$ ($K^0_S \to \pi^0\pi^0$) is the dominant contribution.

8. $B^0 \to J/\psi K^{*0}$ and $B^+ \to J/\psi K^{*+}$

The B^0 is reconstructed from pairs of J/ψ and K^{*0} candidates, while the B^+ uses J/ψ and K^{*+} candidates. Since the combinatoric backgrounds in this mode are larger than in the $B^0 \to J/\psi K^0$ or $B^+ \to J/\psi K^+$ modes, we tighten the particle identification requirements to demand that both J/ψ daughter leptons satisfy either the loose muon selection criteria or tight electron selection criteria.

The distribution of the selected candidates in ΔE and $m_{\rm ES}$ are shown in Figs. 10(c)–10(f).

9. $B^0 \to \psi(2S) K^0_S$ and $B^+ \to \psi(2S) K^+$

Charged B candidates are formed from the combination of a $\psi(2S)$ candidate with a track, and neutral candidates from the combination of $\psi(2S)$ and $K^0_S \to \pi^+\pi^-$ candidates.

In the leptonic decay mode of the $\psi(2S)$, $|\cos\theta_l|$ is required to be less than 0.8. In the J/ψ decay mode of the $\psi(2S)$, $\cos\theta_T$ is required to have an absolute value of less than 0.9. The distribution of the selected candidates in ΔE and $m_{\rm ES}$ is shown in Fig. 11.

10. $B^0 \to \chi_{c1} K^0_S$ and $B^+ \to \chi_{c1} K^+$

$B^0 \to \chi_{c1} K^0_S$ candidates are formed by combining mass-constrained χ_{c1} candidates with mass-constrained $K^0_S \to \pi^+\pi^-$ candidates.

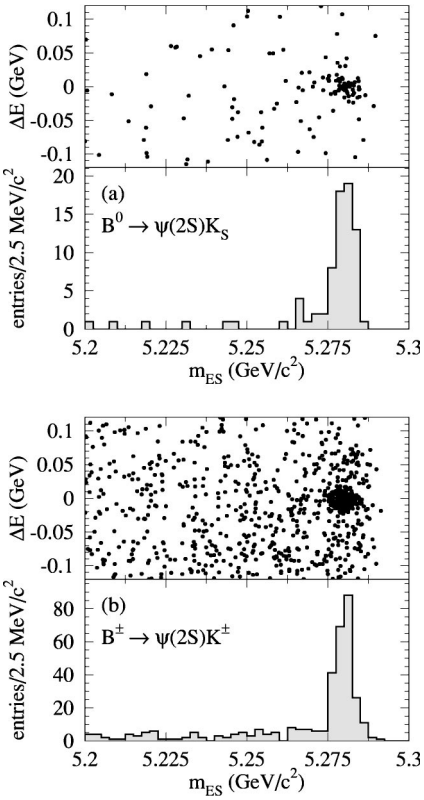

FIG. 11. Signal for (a) $B^0 \to \psi(2S)K_S^0$ and (b) $B^+ \to \psi(2S)K^+$. The upper plots show the distribution of events in the ΔE-$m_{\rm ES}$ plane, and the lower plots show the distribution in $m_{\rm ES}$ of events in the signal region in ΔE.

K^+ candidates are defined as tracks which lie within the angular range $0.35 < \theta < 2.5$ rad. These are combined with mass-constrained χ_{c1} candidates to form $B^+ \to \chi_{c1}K^+$ candidates.

The cosine of the θ_T is required to have absolute value less than 0.9. The distributions of the selected candidates in ΔE and $m_{\rm ES}$ are shown in Figs. 12(a), 12(b).

11. $B^0 \to \chi_{c1}K^{*0}$

B candidates are reconstructed by combining mass-constrained χ_{c1} candidates with K^{*0} candidates reconstructed in the $K^+\pi^-$ mode. We require that the K^+ candidate be inconsistent with a pion hypothesis, using the combined information from dE/dx measured in the SVT and DCH and Cherenkov angle measured in the DIRC. We apply the same particle identification requirements to the J/ψ daughters as are used in the $B^0 \to J/\psi K^{*0}$ and $B^+ \to J/\psi K^{*+}$ selection. χ_{c1} candidates are selected if the mass difference between the χ_{c1} and the J/ψ lies between 0.37 and 0.45 GeV/c^2. K^{*0} candidates are reconstructed using the standard procedure, and are accepted if the K^{*0} mass is within 75 MeV/c^2 of the known value [19].

The distribution of the selected candidates in ΔE and $m_{\rm ES}$ is shown in Fig. 12(c).

VIII. BACKGROUND ESTIMATION

Backgrounds to the decay modes we measure arise predominantly from three sources: other B decays that include charmonium mesons in the final state, B decays without charmonium mesons, and light quark events. Monte Carlo simulation studies verify that for B decays without charmonium mesons and for continuum events, B candidates follow the ARGUS distribution in $m_{\rm ES}$. On the other hand, the background from inclusive charmonium decays includes modes that are kinematically very similar to the signal modes, which means that their distribution in $m_{\rm ES}$ may have a peak in the signal region. As an example, Fig. 13 shows the distribution in ΔE and $m_{\rm ES}$ for signal and background events satisfying the $B^+ \to \chi_{cl}K^+$ selection requirements. It is critical that the so-called ''peaking background'' from other J/ψ modes be well understood, since it contributes directly as a correction to the fitted number of signal events in the signal band.

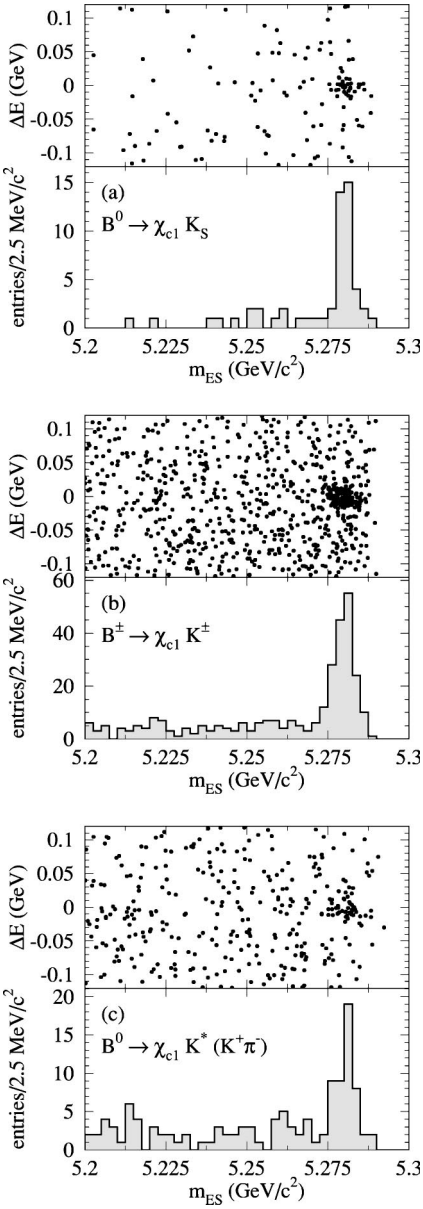

FIG. 12. Signal for (a) $B^0 \to \chi_{c1}K_S^0$, (b) $B^+ \to \chi_{c1}K^+$, and (c) $B^0 \to \chi_{c1}K^{*0}$. The upper plots show the distribution of events in the ΔE-$m_{\rm ES}$ plane, and the lower plots show the distribution in $m_{\rm ES}$ of events in the signal region in ΔE.

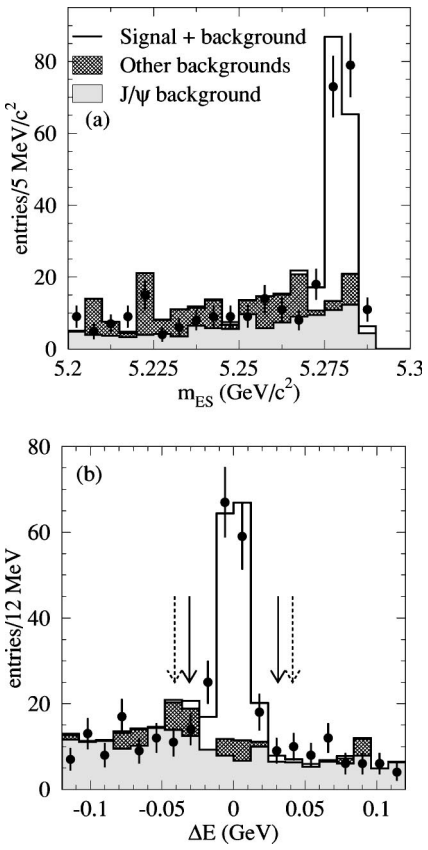

FIG. 13. Distribution in (a) $m_{\rm ES}$ and (b) ΔE of candidates for $B^+ \to \chi_{c1} K^+$. The points are the data, the shaded histograms are Monte Carlo simulated background events, broken down into the combinatorial and inclusive J/ψ contributions, and the open histograms are the sum of the Monte Carlo simulated signal and background distributions. The Monte Carlo distributions are normalized according to the equivalent luminosity of the samples. In (b) the ΔE signal region lies between the solid arrows, and the sideband region in which we compare the observed peaking background to the Monte Carlo prediction lies outside of the dashed arrows. Note that the inclusive J/ψ background peaks in the signal region of $m_{\rm ES}$, but that neither background peaks in the signal region of ΔE.

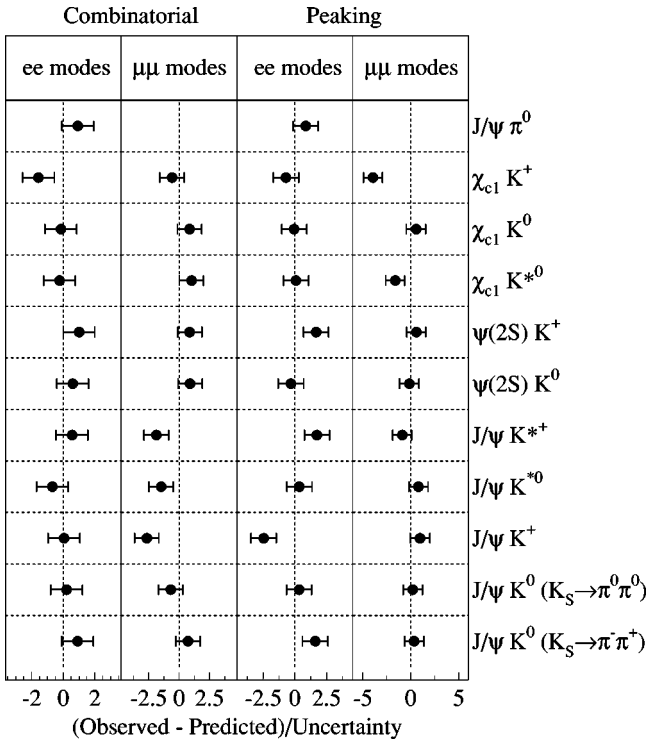

FIG. 14. Difference between the predicted and observed levels of background, divided by the combined statistical error from data and Monte Carlo simulation. The comparison of combinatorial backgrounds is done in the signal region, while for peaking backgrounds the ΔE sideband region is used. For the $J/\psi\pi^0$ mode the value shown is the sum of the e^+e^- and $\mu^+\mu^-$ modes.

For all modes except $B^0 \to J/\psi K^0_L$, we estimate the magnitude of the backgrounds by using Monte Carlo simulation, off-resonance data, and mass sidebands for J/ψ or $\psi(2S)$ candidates in on-resonance data. The available Monte Carlo samples are 10 million $B\overline{B}$ decays, the equivalent of 8 fb^{-1} of continuum events, and the equivalent of several times our data sample of inclusive B to charmonium decays.

We compare the predicted and observed levels of background in two regions of the ΔE-$m_{\rm ES}$ plane: the ΔE sideband, defined as that part of the signal neighborhood sufficiently far from the signal region in $|\Delta E|$ that it contains a negligible amount of signal (typically 4σ from zero, though for modes with a π^0 in the final state this is reduced to 3σ), and the signal region.

In each region, we fit a Gaussian and an ARGUS background distribution to the observed $m_{\rm ES}$ distribution of B candidates in data and Monte Carlo samples. In the ΔE sideband the integral of the Gaussian distribution across the $m_{\rm ES}$ signal region provides an estimate of the peaking background. In the ΔE signal region the integral of the ARGUS background function across the $m_{\rm ES}$ signal region provides an estimate of the combinatorial background. A comparison between data and Monte Carlo simulation of the fitted results for the combinatorial and peaking background components is displayed in Fig. 14. In most cases, the predicted and observed backgrounds are in good agreement, within the statistical errors. Discrepancies in the predicted and observed levels of peaking backgrounds in the ΔE sideband region are accounted for in our estimation of systematic uncertainties.

For the $B^0 \to J/\psi K^0_L$ sample, we estimate the magnitude of the background by performing a binned log-likelihood fit to the $\Delta E_{K^0_L}$ distribution in the range -20 to 80 MeV. This fit is described in detail in Sec. X. The shapes of the signal and inclusive charmonium background components are taken from Monte Carlo simulation. The shape of the noncharmonium background component is taken from an ARGUS fit to the $\Delta E_{K^0_L}$ distribution for events in the J/ψ mass sideband. To constrain the magnitude of this last component, we first estimate the fraction of non-J/ψ candidates in the J/ψ mass window relative to the mass sideband for events with arbitrary $\Delta E_{K^0_L}$. We then scale the number of events with $\Delta E_{K^0_L}$ between -20 and 80 MeV that also have a dilepton invariant mass in the J/ψ sideband region by this fraction to determine the expected number of candidates arising from noncharmonium backgrounds.

TABLE VI. Dominant sources of background in the decay modes we consider, along with the fraction of the total background due to the dominant source. These fractions have substantial uncertainty due to the limited statistics of the available Monte Carlo simulation sample.

Channel		Dominant background	% of total
$B^0 \to J/\psi K^0$	$K^0_S \to \pi^+\pi^-$	Charmonium	70
	$K^0_S \to \pi^0\pi^0$	Continuum $q\bar{q}$	50
	K^0_L	Charmonium	90
$B^+ \to J/\psi K^+$		Charmonium	50
$B^0 \to J/\psi \pi^0$		Continuum $q\bar{q}$	55
$B^0 \to J/\psi K^{*0}$		Charmonium	90
$B^+ \to J/\psi K^{*+}$		Charmonium	85
$B^0 \to \psi(2S) K^0$		Charmonium	60
$B^+ \to \psi(2S) K^+$		Charmonium	50
$B^0 \to \chi_{c1} K^0$		Charmonium	95
$B^+ \to \chi_{c1} K^+$		Charmonium	75
$B^0 \to \chi_{c1} K^{*0}$		Charmonium	90

The dominant source of background for each mode we consider is listed in Table VI.

IX. EFFICIENCY CALCULATION

The selection efficiencies for each mode are obtained from detailed Monte Carlo simulations, in which the detector response is simulated using the GEANT3 [22] program. In addition, we have used the data where possible to determine the detector performance.

We have determined the efficiency for identifying leptons with the sample of inclusively produced J/ψ's in the data. J/ψ's are selected by requiring that one track pass the very tight electron or muon selection, with no lepton identification requirement placed on the other track (the test track). The fraction of test tracks that satisfy a given lepton selection provides a measure of the efficiency for that selection.

We have determined the track finding efficiency from multihadron events in the data. For the standard track selection, the fact that the SVT is an independent tracking device allows precise determination of the DCH efficiency by observing the fraction of tracks in the SVT that are also found in the DCH. For low-momentum pions, such as those produced in the decay $\psi(2S) \to J/\psi \pi^+\pi^-$, D^* decays are used to provide information about the efficiency as a function of momentum. This measurement takes advantage of the correlation between the pion helicity angle in the D^* rest frame and its momentum in the center-of-mass frame. Since the helicity angle distribution is known, any deviation between the expected and observed distributions can be interpreted as arising from a momentum dependence in the track reconstruction efficiency. In addition, the efficiency for reconstructing a $K^0_S \to \pi^+\pi^-$ decay has been determined as a function of the K^0_S flight length from studies of inclusive K^0_S production in the data.

The efficiency for detecting photon clusters has been determined from the data with a control sample of two-prong $\tau^+\tau^-$ events. In the subsample of events tagged by a leptonic decay of one of the taus, we compare the number of events with one or two neutral pions, and one charged pion, from the second tau decay. The ratio of these two branching fractions is known to a precision of 1.6% [19]. By comparing data with simulation, we determine a correction factor to be applied to the photon identification efficiency. This factor is found to be independent of the photon energy.

Both the J/ψ mass distribution and ΔE signal distribution in the $B^+ \to J/\psi K^+$ sample have better resolution in the simulation than in the data, indicating that the track p_T resolution in the simulation is overestimated. To account for this, we degrade the p_T resolution of the simulated tracks by an amount chosen to bring the simulated J/ψ mass and ΔE mass distributions into agreement with those observed in data.

We measure the efficiency of the EMC and the IFR to detect a K^0_L candidate cluster using a control sample of $e^+e^- \to \Phi\gamma$, $\Phi \to K^0_S K^0_L$ events.

The efficiencies of the π^0 veto and missing transverse momentum requirements applied for K^0_L reconstruction in the EMC were determined using $B^+ \to J/\psi K^+$ events.

The $\Delta E_{K^0_L}$ distribution for simulated events is adjusted slightly to account for differences between data and Monte Carlo simulation in the beam energy spread and K^0_L angular resolution. The correction to the beam energy spread is derived from a study of $B^+ \to J/\psi K^+$ events, and the adjustment for the K^0_L angular resolution is determined with the $e^+e^- \to \Phi\gamma$ control sample.

The combination of these effects requires a correction factor to be applied to the efficiency determined from the Monte Carlo simulation. The size of the correction varies among decay modes, and is at most 16%.

X. BRANCHING FRACTION DETERMINATION

To derive branching fractions we have used the secondary branching fractions $\mathcal{S}$ published in Ref. [19]. An exception to this is the branching fraction of $\psi(2S) \to l^+l^-$, where we have used our recent measurement of $(6.6 \pm 1.1) \times 10^{-3}$ [23] for the $\psi(2S) \to \mu^+\mu^-$ mode and the measurement from E835 [24] for the $\psi(2S) \to e^+e^-$ mode. These measurements are more recent and more accurate than those included in Ref. [19].

We have assumed that $\Upsilon(4S)$ decays produce an equal mixture of charged and neutral B mesons. The dependence of our results on this assumption is included in Sec. XII.

For all modes except $B^0 \to J/\psi K^0_L$, $B^0 \to J/\psi K^{*0}$ and $B^+ \to J/\psi K^{*+}$, the number of signal events N_s within the signal region of the ΔE-$m_{\rm ES}$ plane is determined from the observed number of events after background subtraction. The background has two components, as described in Sec. VIII: a combinatorial component, which is obtained by integrating the fitted ARGUS distribution in the signal region, and a peaking component that is obtained from inclusive $B \to J/\psi X$ simulation after removing the signal channel. The procedure is illustrated in Fig. 15.

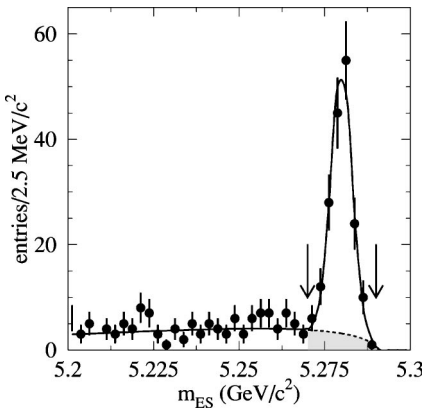

FIG. 15. Distribution in $m_{\rm ES}$ of candidates for $B^+\to\chi_{c1}K^+$, with the ARGUS and Gaussian fit superimposed. The number of signal events is calculated by counting the events in the signal region of $m_{\rm ES}$ (marked by arrows) and subtracting the integral of the fit ARGUS function across this region (the shaded portion of the fit) and the peaking contribution from inclusive J/ψ backgrounds, as shown in Fig. 13.

We determine the branching fraction by dividing N_s by the selection efficiency ϵ, $\mathcal{S}$, and the number of $B\overline{B}$ events in the sample $N_{B\overline{B}}$. Where possible, the branching fraction is determined independently for the different secondary decay modes, and the results combined statistically, taking into account correlations in the systematic errors. For the channels that are statistically limited, we determine the branching fraction using the combined sample of candidate B events, irrespective of the secondary decay mode,

$$\mathcal{B}=\frac{\sum_i N_{s,i}}{N_{B\overline{B}}\sum_i \epsilon_i\mathcal{S}_i}, \tag{5}$$

where the sum is over all decay modes considered.

The branching fractions for the $B^0\to J/\psi K^{*0}$ ($\mathcal{B}^0$) and $B^+\to J/\psi K^{*+}$ ($\mathcal{B}^+$) modes are determined simultaneously from a likelihood fit, which is required to account for the crossfeed between the K^* decay channels. The cross feed is largest for the mode $B^+\to J/\psi K^{*+}$, where the K^{*+} decays to $K^+\pi^0$. In this case, 12% of the selected candidates arise from other $B\to J/\psi\ K^*$ decays. The likelihood function includes the cross-feed contributions as well as all other background sources, and has the form

$$\mathcal{L}(\mathcal{B}^0,\mathcal{B}^+)=\prod_{i,j}\frac{\mu_{ij}^{N_{ij}}e^{-\mu_{ij}}}{N_{ij}!} \tag{6}$$

where i represents a decay mode of the K^* (to K_S^0 or K^+), j represents either the $B^0\to J/\psi K^{*0}$ or $B^+\to J/\psi K^{*+}$ mode, N is the observed number of events in the signal region, and μ is the expected number of events. The last is given by

$$\mu_{ij}=N_{b,ij}+\sum_{i'j'}\mathcal{B}^{j'}\epsilon_{iji'j'}\mathcal{S}_{i'j'}N_{B\overline{N}} \tag{7}$$

where N_b is the number of background events estimated in the same manner as for the other channels. The four indices attached to the selection efficiencies denote the fraction of events in the $i'j'$ mode that pass the ij selection requirements, as determined with the Monte Carlo simulation.

We determine the number of signal and background events for the $B^0\to J/\psi K_L^0$ decay mode by performing a binned likelihood fit to the $\Delta E_{K_L^0}$ distribution. The fit takes as input a_i, the fraction of simulated $B^0\to J/\psi K_L^0$ events in the ith bin, b_i, the fraction of simulated inclusive charmonium background events in the ith bin, c_i, the fraction of noncharmonium background events from the mass sidebands of the J/ψ in the ith bin, and d_i, the number of data events in the ith bin. The likelihood function has the form

$$\mathcal{L}(N_s,N_{\psi X},N_{\text{non-}\psi})=\prod_{i=1}^{N_{\rm bin}}\frac{\mu_i^{d_i}e^{-\mu_i}}{d_i!}\times\frac{e^{-(N_{\text{non-}\psi}-M)^2/2(\sigma^2+N_{\text{non-}\psi})}}{\sqrt{2\pi(\sigma^2+N_{\text{non-}\psi})}} \tag{8}$$

where $N_{\psi X}$ is the number of inclusive charmonium background events, $N_{\text{non-}\psi}$ is the number of noncharmonium background events, M is the expected number of noncharmonium background events determined from the mass sidebands of the J/ψ, σ is the uncertainty on M, and μ_i is the expected number of events in the ith bin, defined as

$$\mu_i\equiv N_s a_i+N_{J/\psi X}b_i+N_{\text{non-}\psi}c_i\,. \tag{9}$$

XI. SYSTEMATIC ERRORS

Systematic errors on the results arise from the uncertainty on the number of $B\overline{B}$ events, the secondary branching fractions of the modes considered, the estimate of the selection efficiency and the knowledge of the background level. The size of the various contributions to the systematic error, expressed as a fraction of the branching fraction value, is listed for all modes except $B^0\to J/\psi K_L^0$ in Table VII and for the $B^0\to J/\psi K_L^0$ mode in Table VIII. In some cases, a given channel is assigned a much larger uncertainty than other channels for the same effect. This reflects the size of the sample available to evaluate the uncertainty in that mode, and does not mean that the channel is known to have a greater sensitivity to the effect considered.

The uncertainty on the number of $B\overline{B}$ events introduces a systematic error of 1.6% in common for all modes. The uncertainties in the branching fractions of the secondary decay modes lead to a systematic error of between 1.7% and 9.8%, depending on the mode considered.

The systematic error due to the finite size of the available Monte Carlo sample is between 0.1% and 2.4% for the different modes.

TABLE VII. Breakdown of contributions to the systematic errors. Included are the contributions from the secondary branching fractions ($\mathcal{S}$), lepton identification efficiency (PID), track p_T resolution (Trk p_T), track and $K^0_S \to \pi^+\pi^-$ reconstruction efficiency [ϵ(Trk+K^0_S)], photon identification efficiency [$\epsilon(\gamma)$], background determination (BGR), Monte Carlo statistics ($N_{\rm sim}$) and selection requirement variation (Sel. var.). The 1.6% error from the determination of the number of $B\overline{B}$ events, which is common to all modes, is not listed but is included in the total. In addition, the statistical uncertainty is shown. All values are expressed relative to the measured branching fraction, in percent.

Channel		$\mathcal{S}$	PID	Trk p_T	ϵ(Trk+K^0_S)	$\epsilon(\gamma)$	BGR	$N_{\rm sim}$	Sel. var.	Total	Stat. error
$B^0 \to J/\psi K^0$	$K^0_S \to \pi^+\pi^-$	1.7	1.3	0.9	5.5	-	1.1	1.3	3.5	7.3	6.4
	$K^0_S \to \pi^0\pi^0$	1.7	0.5	0.1	2.4	5.0	2.0	1.6	2.5	7.0	15.2
$B^+ \to J/\psi K^+$		1.7	1.4	1.0	3.6	-	1.0	0.8	2.2	5.3	3.1
$B^0 \to J/\psi \pi^0$		1.7	2.5	0.4	2.4	2.5	1.7	1.1	10.0	11.3	32.7
$B^0 \to J/\psi K^{*0}$		1.7	1.3	0.8	4.7	0.2	1.4	0.2	4.0	6.9	4.0
$B^+ \to J/\psi K^{*+}$		1.7	1.3	1.1	4.9	1.2	2.9	0.1	5.0	8.2	6.6
$B^0 \to \psi(2S) K^0$		9.6	1.0	1.3	7.9	-	4.8	1.4	8.5	15.9	15.4
$B^+ \to \psi(2S) K^+$		9.6	1.0	1.3	5.8	-	1.3	1.6	3.7	12.1	8.1
$B^0 \to \chi_{c1} K^0$		6.2	2.4	1.2	5.6	1.3	14.5	2.2	13.2	22.0	25.1
$B^+ \to \chi_{c1} K^+$		6.1	2.6	0.5	3.6	1.8	3.8	2.4	5.3	10.6	10.0
$B^0 \to \chi_{c1} K^{*0}$		6.2	2.4	0.8	4.8	2.7	14.3	1.8	8.1	18.7	28.8

We have determined the efficiency for a charged particle to be reconstructed as a track that passes the standard track selection to a precision of 1.2% per track. The uncertainty in the reconstruction efficiency for the low-momentum pions from the $\psi(2S) \to J/\psi \pi^+\pi^-$ decay is determined to be 2% per track. The systematic error associated with reconstructing a $K^0_S \to \pi^+\pi^-$ decay has two sources: knowledge of the reconstruction efficiency for the two π tracks, and differences in the selection criteria efficiencies observed between the inclusive K^0_S data and the Monte Carlo simulation. The observed discrepancies and their statistical uncertainties are summed in quadrature to yield a systematic error of approximately 5%.

The systematic error on lepton identification efficiencies arise from the statistics of the inclusive J/ψ sample, and from comparing the efficiencies in different low-multiplicity control samples. It varies from 0.5 to 2.8 % per J/ψ or $\psi(2S)$ depending on the criteria used to select the leptons.

The quality of the simulation of photon detection and energy measurement in the EMC has been validated by a detailed comparison between real and simulated data. In particular, the position and resolution of the π^0 and η mass peaks in the photon pair mass spectrum has been compared as function of photon energy, calorimeter occupancy and time of data collection. The agreement in terms of energy scale is found to be better than 0.75% in all cases; energy resolution is also well described at the level of 1.5%. The absolute photon detection efficiency is known to 1.25%. The resulting systematic errors on the branching fractions are in the range of 1.3 to 5% depending on the decay mode.

We account for the uncertainty in the p_T resolution by varying the amount by which the Monte Carlo simulated momentum resolution is degraded within the range in which the data and Monte Carlo J/ψ mass and ΔE widths are compatible. The observed variation in selection efficiency is between 0.1% and 1.3%. To account for the possibility that other variables used in selecting candidates may not be perfectly modeled in the simulation, we vary the selection requirements and repeat the branching fraction measurement. In most cases the range of variation is $\pm 1\sigma$, where σ is the width observed in data for the variable under consideration, while for helicity angles a variation of ± 0.05 in their cosine is used. The observed variations in the results are between 2.2% and 13.2%. Modes with a K^* in the final state merit special mention, since there can be some variation of selection efficiency with the polarization of the vector meson, and the polarization amplitudes are subject to experimental uncertainty. The Monte Carlo simulation from which we derive our efficiency assumes the polarization amplitudes measured by CLEO [25]. We have studied the changes in efficiency that occur when the amplitudes are varied by twice the difference between the values measured at CLEO and *BABAR*

TABLE VIII. Breakdown of contributions to the systematic error for the $B^0 \to J/\psi K^0_L$ analysis. The statistical error is also shown, with all values expressed relative to the measured branching fraction, in percent.

Source	Uncertainty
Tracking efficiency	2.4
Lepton identification efficiency	1.2
J/ψ mass requirement efficiency	1.3
K_L efficiency	9
π^0 veto efficiency	0.7
Missing momentum requirement efficiency	0.5
Beam energy scale (spread)	1.0 (3.0)
K_L angular resolution	4
Branching fractions for $B \to J/\psi$ X	3.8
non-J/ψ background shape	2
Simulation statistics	2.2
Secondary branching fractions	1.2
Number of $B\overline{B}$ events	1.6
Total	12.0
Statistical error	12.0

[13]. We find that these changes are consistent with those observed when the selection requirement on θ_K is varied.

For the $B^0 \to J/\psi K_L^0$ analysis, we include additional systematic errors associated with the selection efficiency. These originate from the uncertainty in the K_L^0 reconstruction efficiency and angular resolution determined from data, the knowledge of the absolute scale and spread of the beam energy, and from the various selection requirements used to isolate the signal.

Another systematic error arises from our knowledge of the backgrounds. For all modes except $B^0 \to J/\psi K_L^0$, we use data in the ΔE sideband to estimate this uncertainty. We determine the uncertainty in the size of the combinatorial background by repeating the fit to the data with the shape of the ARGUS function [the parameter c in Eq. (4)] fixed to the value obtained from fitting the ΔE sidebands, allowing only the normalization to vary. This accounts for any correlation between the ARGUS and Gaussian fits in the ΔE signal region. We estimate the uncertainty in the predicted size of the peaking background by comparing the observed Gaussian component in the ΔE sideband to that estimated from the inclusive $B \to J/\psi X$ simulation. This procedure takes advantage of the fact that the distribution of candidates from this background in ΔE depends primarily on kinematics rather than the poorly, known composition of the background. In particular, the background does not peak in the signal region of ΔE (see Fig. 13), which implies that the relative normalization observed in the ΔE sideband can also be expected to hold in the signal region. The systematic error attributed to the knowledge of the backgrounds varies from 1.0 to 14.5 % for the various modes. In addition, for the $B^0 \to J/\psi K^{*0}$, $B^+ \to J/\psi K^{*+}$ and $B^0 \to \chi_{c1} K^{*0}$ modes, a systematic error is included to account for the uncertainty in the nonresonant $B \to J/\psi K \pi$ branching fractions, and the contribution of feed down from higher K^* resonances. This ranges from 1.4 to 3.7 % depending on the mode.

For the $B^0 \to J/\psi K_L^0$ decay mode, we determine the uncertainty arising from knowledge of the shape of the non-J/ψ background both by changing the fitted parameters of the ARGUS function for this background component by one standard deviation and also directly in the fit by using the $\Delta E_{K_L^0}$ distribution from the non-J/ψ events in the data. The analysis is also repeated after varying the values of the branching fractions for the component modes in the simulation of $B \to J/\psi X$ decays by the uncertainty quoted in Ref. [19]. This is done separately for the main background modes and then for all the remaining modes together. Since the nonresonant $B \to J/\psi K \pi$ component is poorly measured, we vary it in the range from -50 to $+400$ %.

XII. RESULTS

In Table IX we summarize our branching fraction measurements. The observed number of events in the signal region, the predicted background, and the selection efficiency are given in Table X.

From these results, we have determined the following ratios of charged to neutral branching fractions, where the first error is statistical and the second systematic:

TABLE IX. Measured branching fractions for exclusive decays of B mesons involving charmonium. The first error is statistical and the second systematic.

Channel		Branching fraction/10^{-4}
$B^0 \to J/\psi K^0$	$K_S^0 \to \pi^+\pi^-$	8.5 ± 0.5 ± 0.6
	$K_S^0 \to \pi^0\pi^0$	9.6 ± 1.5 ± 0.7
	K_L^0	6.8 ± 0.8 ± 0.8
	All	8.3 ± 0.4 ± 0.5
$B^+ \to J/\psi K^+$		10.1 ± 0.3 ± 0.5
$B^0 \to J/\psi \pi^0$		0.20 ± 0.06 ± 0.02
$B^0 \to J/\psi K^{*0}$		12.4 ± 0.5 ± 0.9
$B^+ \to J/\psi K^{*+}$		13.7 ± 0.9 ± 1.1
$B^0 \to \psi(2S) K^0$		6.9 ± 1.1 ± 1.1
$B^+ \to \psi(2S) K^+$		6.4 ± 0.5 ± 0.8
$B^0 \to \chi_{c1} K^0$		5.4 ± 1.4 ± 1.1
$B^+ \to \chi_{c1} K^+$		7.5 ± 0.8 ± 0.8
$B^0 \to \chi_{c1} K^{*0}$		4.8 ± 1.4 ± 0.9

$$\frac{\mathcal{B}(B^+ \to J/\psi K^+)}{\mathcal{B}(B^0 \to J \psi K^0)} = 1.20 \pm 0.07 \pm 0.04 \tag{10}$$

$$\frac{\mathcal{B}(B^0 \to J/\psi K^{*+})}{\mathcal{B}(B^0 \to J/\psi K^{*0})} = 1.10 \pm 0.09 \pm 0.08 \tag{11}$$

$$\frac{\mathcal{B}(B^+ \to (2S) K^+)}{\mathcal{B}(B^0 \to \psi(2S) K^0)} = 0.94 \pm 0.16 \pm 0.10 \tag{12}$$

$$\frac{\mathcal{B}(B^+ \to \chi_{cl} K^+)}{\mathcal{B}(B^0 \to \chi_{c1} K^0)} = 1.39 \pm 0.37 \pm 0.22. \tag{13}$$

Combining all of these measurements yields

$$\frac{\mathcal{B}(B^+ \to \text{charmonium})}{\mathcal{B}(B^0 \to \text{charmonium})} = 1.17 \pm 0.07 \pm 0.04. \tag{14}$$

Assuming equal partial widths for $B^0 \to J/\psi h^0$ and $B^+ \to J/\psi h^+$ for any meson h and using the known ratio of the charged to neutral B meson lifetimes $\tau_{B^+}/\tau_{B^0} = 1.062 \pm 0.029$ [19], we find

$$R^{+/0} \equiv \frac{\mathcal{B}(\Upsilon(4S) \to B^+ B^-)}{\mathcal{B}(\Upsilon(4S) \to B^0 \overline{B}^0)} = 1.10 \pm 0.06 \pm 0.05. \tag{15}$$

We provide the formulas for recomputing our results for an arbitrary value of $R^{+/0}$, rather than the value of unity we have assumed:

$$\mathcal{B}(B^+ \to X, R^{+/0}) = \frac{(1 + R^{+/0})}{2R^{+/0}} \mathcal{B}(B^+ \to X, 1) \tag{16}$$

$$\mathcal{B}(B^0 \to X, R^{+/0}) = \frac{(1 + R^{+/0})}{2} \mathcal{B}(B^0 \to X, 1). \tag{17}$$

TABLE X. The observed number of events in the signal region, estimated background, efficiency, efficiency times secondary branching fractions, and measured branching fraction for exclusive decays of B mesons involving charmonium. The combinatorial background is estimated from a fit to the signal plus sideband region in $m_{\rm ES}$, while the peaking background is estimated with Monte Carlo. For the $B^0 \to J/\psi K_L^0$ mode the inclusive charmonium background is listed in the "Peaking" column and the other backgrounds in the "Combinatorial" column. For the branching fractions, the first error is statistical and the second systematic.

Channel		$N_{\rm obs}$	Combinatorial Bkgr	Peaking Bkgr	Efficiency (%)	Eff$\times\mathcal{S}$(%)	Branching fraction/10^{-4}
$B^0 \to J/\psi K^0$	$K_S^0 \to \pi^+\pi^-$	275	6.1 ± 2.7	3.4 ± 1.1	33.8	1.37	$8.5 \pm 0.5 \pm 0.6$
	$K_S^0 \to \pi^0\pi^0$	77	12.2 ± 3.7	2.3 ± 0.9	15.5	0.29	$9.6 \pm 1.5 \pm 0.7$
	K_L^0	408	25 ± 3	200 ± 14	22.3	1.46	$6.8 \pm 0.8 \pm 0.8$
	All						$8.3 \pm 0.4 \pm 0.5$
$B^+ \to J/\psi K^+$		1135	8.9 ± 2.6	17.1 ± 2.6	41.2	4.86	$10.1 \pm 0.3 \pm 0.5$
$B^0 \to J/\psi \pi^0$		19	4.7 ± 0.9	0.7 ± 0.1	25.8	3.01	$0.20 \pm 0.06 \pm 0.02$
$B^0 \to J/\psi K^{*0}$		695	50.2 ± 7.8	50.0 ± 3.3	22.6	1.10	$12.4 \pm 0.5 \pm 0.9$
$B^+ \to J/\psi K^{*+}$		625	160.6 ± 15.9	87.0 ± 5.8	17.9	1.09	$13.7 \pm 0.9 \pm 1.1$
$B^0 \to \psi(2S) K^0$		63	6.0 ± 3.3	1.0 ± 0.8	22.0	0.37	$6.9 \pm 1.1 \pm 1.1$
$B^+ \to \psi(2S) K^+$		247	27.2 ± 5.5	12.5 ± 2.8	29.6	1.46	$6.4 \pm 0.5 \pm 0.8$
$B^0 \to \chi_{c1} K^0$		37	7.2 ± 2.1	3.7 ± 1.3	19.1	0.21	$5.4 \pm 1.4 \pm 1.1$
$B^+ \to \chi_{c1} K^+$		179	24.2 ± 4.7	9.7 ± 2.7	26.3	0.85	$7.5 \pm 0.8 \pm 0.8$
$B^0 \to \chi_{c1} K^{*0}$		52	13.0 ± 1.6	6.4 ± 5.8	13.9	0.30	$4.8 \pm 1.4 \pm 0.9$

We also determine the ratio of branching fractions for a vector versus scalar light meson accompanying the charmonium meson:

$$\frac{\mathcal{B}(B^0 \to J/K^{*0})}{\mathcal{B}(B^0 \to J/\psi K^0)} = 1.49 \pm 0.10 \pm 0.08 \tag{18}$$

$$\frac{\mathcal{B}(B^+ \to J/\psi K^{*+})}{\mathcal{B}(B^+ \to J/\psi K^+)} = 1.37 \pm 0.10 \pm 0.08 \tag{19}$$

$$\frac{\mathcal{B}(B^0 \to \chi_{c1} K^{*0})}{\mathcal{B}(B^0 \to \chi_{c1} K^0)} = 0.89 \pm 0.34 \pm 0.17. \tag{20}$$

These three ratios are consistent and yield an average value:

$$\frac{\mathcal{B}(B \to \text{charmonium} + \text{vector})}{\mathcal{B}(B \to \text{charmonium} + \text{scalar})} = 1.40 \pm 0.07 \pm 0.06. \tag{21}$$

Finally, the following ratios between the production rates for different charmonium states have been determined:

$$\frac{\mathcal{B}(B^0 \to \psi(2S) K^0)}{\mathcal{B}(B^0 \to J/\psi K^0)} = 0.82 \pm 0.13 \pm 0.12 \tag{22}$$

$$\frac{\mathcal{B}(B^0 \to \chi_{c1} K^0)}{\mathcal{B}(B^0 \to J/\psi K^0)} = 0.66 \pm 0.11 \pm 0.17 \tag{23}$$

$$\frac{\mathcal{B}(B^+ \to \psi(2S) K^+)}{\mathcal{B}(B^+ \to J/\psi K^+)} = 0.64 \pm 0.06 \pm 0.07 \tag{24}$$

$$\frac{\mathcal{B}(B^+ \to \chi_{c1} K^+)}{\mathcal{B}(B^2 \to J/\psi K^+)} = 0.75 \pm 0.08 \pm 0.05. \tag{25}$$

XIII. SUMMARY

We have presented measurements of branching fractions of B mesons to several two-body final states that include a $J/\psi, \psi(2S)$ or χ_{c1} meson and a K^0, K^+, K^* or π^0. Our results are in good agreement with previous measurements [19] and have superior precision, both in terms of individual branching fractions and their ratios. In addition, based on isospin invariance, we find the ratio of charged to neutral B meson production on the $\Upsilon(4S)$ resonance to be compatible with unity within two standard deviations, and also compatible with the measurement reported by CLEO [26]. Our central value and CLEOs are both higher than one, with the difference in our case larger than one standard deviation.

ACKNOWLEDGMENTS

We are grateful for the extraordinary contributions of our PEP-II colleagues in achieving the excellent luminosity and machine conditions that have made this work possible. The collaborating institutions wish to thank SLAC for its support and the kind hospitality extended to them. This work is supported by the U.S. Department of Energy and National Science Foundation, the Natural Sciences and Engineering Research Council (Canada), Institute of High Energy Physics (China), the Commissariat à l'Energie Atomique and Institut National de Physique Nucléaire et de Physique des Particules (France), the Bundesministerium für Bildung und Forschung (Germany), the Istituto Nazionale di Fisica Nucleare (Italy), the Research Council of Norway, the Ministry of Science and Technology of the Russian Federation, and the Particle Physics and Astronomy Research Council (United Kingdom). Individuals have received support from the Swiss National Science Foundation, the A. P. Sloan Foundation, the Research Corporation, and the Alexander von Humboldt Foundation.

[1] BABAR Collaboration, B. Aubert *et al.*, Phys. Rev. Lett. **86**, 2515 (2001).
[2] M. Wirbel, B. Stech, and M. Bauer, Z. Phys. C **29**, 637 (1985); **34**, 103 (1987).
[3] N. Isgur and M. B. Wise, Phys. Lett. B **232**, 113 (1989); **237**, 527 (1990).
[4] M. Neubert, V. Rieckert, B. Stech, and Q. P. Xu, in *Heavy Flavours*, edited by A. J. Buras and M. Lindner (World Scientific, Singapore, 1992), p. 286.
[5] A. Deandrea, N. Di Bartolomeo, R. Gatto, and G. Nardulli, Phys. Lett. B **318**, 549 (1993); A. Deandrea *et al.*, *ibid.* **320**, 170 (1994).
[6] R. Aleksan *et al.*, Phys. Rev. D **51**, 6235 (1995).
[7] M. Neubert and B. Stech, in *Heavy Flavours II*, edited by A. J. Buras and M. Lindner (World Scientific, Singapore, 1998), p. 345.
[8] M. Ciuchini *et al.*, Nucl. Instrum. Methods Phys. Res. A **408**, 28 (1998); Eur. Phys. J. C **9**, 43 (1999).
[9] M. Gourdin, Y. Y. Keum, and X. Y. Pham, Phys. Rev. D **52**, 1597 (1995).
[10] T. W. Yeh and H. Li, Phys. Rev. D **56**, 1615 (1997).
[11] M. Ciuchini *et al.*, Eur. Phys. J. C **9**, 43 (1999).
[12] H. Y. Cheng and K. C. Yang, Phys. Rev. D **63**, 074011 (2001).
[13] BABAR Collaboration, B. Aubert *et al.*, Phys. Rev. Lett. **87**, 241801 (2001).
[14] BABAR Collaboration, B. Aubert *et al.*, ''Measurement of the ratio of the branching fractions $\mathcal{B}(B^+\rightarrow J/\psi\pi^+)/\mathcal{B}(B^+\rightarrow J/\psi K^+)$,'' SLAC-PUB-8942, hep-ex/0108009 (in preparation).
[15] BABAR Collaboration, B. Aubert *et al.*, ''The BABAR detector,'' SLAC-PUB-8569, hep-ex/0105044.
[16] A. Drescher *et al.*, Nucl. Instrum. Methods Phys. Res. A **237**, 464 (1985).
[17] R. Sinkus and T. Voss, Nucl. Instrum. Methods Phys. Res. A **391**, 360 (1997).
[18] G. C. Fox and S. Wolfram, Nucl. Phys. **B149**, 413 (1979).
[19] Particle Data Group, D. E. Groom *et al.*, Eur. Phys. J. C **15**, 1 (2000).
[20] BES Collaboration, J. Z. Bai *et al.*, Phys. Rev. D **62**, 032002 (2000).
[21] ARGUS Collaboration, H. Albrecht *et al.*, Phys. Lett. B **185**, 218 (1987); **241**, 278 (1990).
[22] ''GEANT, Detector Description and Simulation Tool,'' CERN program library long writeup W5013, 1994.
[23] BABAR Collaboration, B. Aubert *et al.*, ''Measurement of the branching fractions $\psi(2S)\rightarrow e^+e^-$ and $\psi(2S)\rightarrow\mu^+\mu^-$,'' SLAC-PUB-8953, hep-ex/0109004.
[24] E835 Collaboration M. Ambrogiani *et al.*, Phys. Rev. D **62**, 032004 (2000).
[25] CLEO Collaboration, C. P. Jessop *et al.*, Phys. Rev. Lett. **79**, 4533 (1997).
[26] CLEO Collaboration, J. P. Alexander *et al.*, Phys. Rev. Lett. **86**, 2737 (2001).